Front. Phys. China, 2009, 4(3): 337–355
DOI 10.1007/s11467-009-0038-2

REVIEW ARTICLE

Density functional theory study of surface catalysis and adsorption on several elements in Group I-B and VIII

Wang GAO (高旺), **Qing JIANG** (蒋青)(✉)

Key Laboratory of Automobile Materials (Ministry of Education), and Department of Materials Science and Engineering, Jilin University, Changchun 130022, China
E-mail: jiangq@jlu.edu.cn

Received January 7, 2009; accepted February 28, 2009

This review deals with the high-throughput field in surface catalysis and adsorption. Special focus is placed on advanced methods for knowledge discovery such as density functional theory (DFT) simulations. An inventory of successful cases on several elements in Group I-B and VIII is reported, including the relevant data and knowledge management, which are very important in chemical industry, fuel cell, and environment protection, for both scientific and economical reasons.

Keywords density functional theory, ethylene epoxidation, benzene dehydrogenation, acetylene, methanol, carbon monoxide

PACS numbers 02.70.-c

Contents

1 Introduction

1.1 Scope

This report starts with a brief overview of the surface catalysis and adsorption of elements in Group I-B and VIII. Deeper and consistent insight into these catalytic mechanisms is of fundamentally great importance for advancing catalyst applications. In Section 2, density functional theory (DFT) simulations are introduced. Section 3 develops these methods to research some of catalytic reactions: ethylene epoxide on Ag surface, dehydrogenation of benzene on Cu(100) and Pt(111), oxidation of methanol on Pt(111), some of precursory studies for catalysis – the adsorption of CO on surfaces of 4*d* and 5*d* elements in Group VIII and Cu clusters, and C_2H_2 adsorbed on Cu surface. Comparisons of calculations with available experimental evidences and other simulations are also presented in the corresponding section. Section 4 summarizes the main contributions and limitations of these simulation works, with suggestions for future directions in extending the developed knowledge and associated approaches.

1.2 Overview

Over 80% of commercial chemical processes involve the use of catalysis, with products as varied as chemicals, oil products, fertilizers, plastics, drugs, and pharmaceuticals being made through catalytic steps. Catalysis is probably the most important means of producing modern chemicals. Precious metal catalyst is one kind of the deepest and intensively researched catalysts that have

been widely used in chemical industry, fuel cell technology, environment protection, etc., such as ammonia oxidation (Pt, Au, and Ag) [1–5], hydrogenation (Ni, Pt, Ph, Ir, Ru, ...) [6–9], hydrogenolysis (Os, Ru, Ni, ...) of organic compounds [10–12], ethylene epoxidation (Ag) [13–17], hydrogenation of CO (Fe, Co, ...) [18], and purification of automotive exhaust gases [19, 20]. Nearly all the precious metals can be used as catalysts, usually Pt, Pd, Rh, Ag, and Ru, especially Pt and Rh. Their *d*-orbits are not fully filled. Moreover, their surfaces can adsorb reactants easily, with moderate bonding strength, which are propitious to form the "intermediate". Meanwhile, they own anti-high temperature, anti-oxidation, and corrosion-resistant properties. These make them the most important catalytic materials.

However, there are also many problems about the catalytic mechanism and the processes that limit the application and development of the catalysts. The way to reach a microscopic understanding of the sequence of elementary steps by which a product is formed is to isolate and identify the intermediates. These intermediates are thermodynamically and kinetically accessible using traditional surface science techniques, such as temperature-programmed desorption (TPD) and high-resolution electron energy loss spectroscopy (HREELS). Quantum mechanical computational tools, such as DFT, may then be used to construct a reaction coordinate that is in accordance with experimental observations. This approach allows the determination of not only the surface intermediates but also the relevant transition states (TSs) along the reaction coordinate. The understanding of surface–adsorbate interactions in this way, with the adsorbates being either surface intermediates or TSs, is crucial in the design of new or improved catalysts from first principles.

2 Principle

In 1960s, DFT was proposed by Hohenberg and Kohn [21] and Kohn and Sham [22]. The fundamental proof of DFT is the existence of a local, effective mean field potential, V_{eff}, which depends on only the electron density. Now, many software include DFT calculation code, such as MS modeling and VASP [23]. In MS modeling, there are CASTEP and DMol^3 codes [24–26]. CASTEP is a program based on total energy plane-wave pseudopotential methods, which employs DFT to simulate the properties of solids, interfaces, and surfaces for a wide range of material classes [27]. Owing to its unique approach to electrostatics, DMol^3 has long been one of the fastest methods for molecular DFT calculations and can quickly perform structure optimizations of molecular systems using delocalized internal coordinates [27]. DMol^3 can also be used to search very efficiently for TSs using a combination of linear synchronous transit (LST)/quadratic synchronous transit (QST) algorithms with conjugate gradient refinement, thereby avoiding the computationally expensive calculation of the Hessian matrix. The exchange-correlation functionals are consisted of the generalized gradient approximation (GGA) and local density approximation (LDA).

Exploring the potential energy surface of any reaction requires both structural and energetic, or kinetic and thermodynamic, snapshots of each step in the reaction process. Of particular importance is the rate-determining step, which usually involves finding the elusive TS structure. A few techniques have been well validated for finding a transition-state structure, and among the better known of these are LST/QST and nudged elastic band (NEB) [28]. The NEB method introduces a fictitious spring force that connects neighboring points on the path to ensure continuity of the path and projection of the force so that the system converges to the minimum energy path (MEP). The NEB method has been widely used in solid-state physics and has recently been applied to molecules as well. The advantage of the NEB algorithm is that it provides a fast qualitative examination of the global MEP rather than the locally restricted one and is thus more reliable than the constrained optimization method sometimes used for time-consuming reasons. In particular, the constrained optimization method may overestimate activation barriers as pointed out in a recent DFT study on water dissociation [29].

3 Application: case studies

3.1 Chemical industry

3.1.1 Ethylene epoxidation

Ethylene epoxidation is one of the major petrochemical processes converting several billion US dollars annually due to the importance of ethylene oxide as a versatile chemical intermediate. It is also one of the most important heterogeneous catalytic oxidation processes. There are many features of ethylene epoxidation that have puzzled scientists for decades. Surprisingly, silver is an exceptional catalyst material for ethylene epoxidation. To the best of our knowledge, no other materials come even close to producing the epoxidation activity and selectivity of silver under practical conditions. However, it is shown that copper in UHV is an even more selective epoxidation catalyst than silver [30, 31]. Unfortunately, an inactivating oxide overlayer is formed on copper in the presence of gas-phase oxygen [30, 31]. Many scientists believe that the interaction between oxygen and silver plays an essential role in understanding ethylene epoxidation and a great research effort has been devoted

to the silver–oxygen system [32, 33]. However, the form and the creation of the active oxygen species are still debated.

From now on, it is impossible to study ethylene epoxidation directly in UHV by surface science techniques presumably because ethylene and/or the active oxygen species desorb before the reaction barrier can be climbed. This is probably the main reason that the mechanism remains controversial. However, intermediates such as molecular oxygen [34, 35], atomic oxygen [34, 36–39], subsurface/dissolved oxygen [40, 41], ethylene [42], ethylene oxide [42, 43], acetaldehyde [44], water [45], carbon dioxide [46], and oxametallacycles [47, 48] have been studied by surface science techniques. Furthermore, to understand the sequence of the elementary steps to form C_2H_4O, isolating and identifying intermediates are thermodynamically and kinetically accessible using different surface science techniques, such as TPR [40, 49, 50], pulse reactors [50], batch reactors [51], combining high-pressure cells with UHV techniques [52] and "frozen in time" [53], temperature-programmed desorption and high-resolution election energy loss spectroscopy [13], and DFT calculations with a total energy minimization technique.

The early research is much concerned with the question of whether molecular or atomic adsorbed oxygen reacts with ethylene to form ethylene oxide [54, 55]. Experimental results indicate that atomic oxygen is the active species. Furthermore, it has been discussed whether an Eley–Rideal or a Langmuir–Hinshelwood type of mechanism is appropriate to describe the process [32]. It is also suggested that the active phase of the catalyst is not metallic silver but a surface oxide [56]. This explains the low stability of the active oxygen compared to ethylene, the increasing selectivity with O_2:C_2H_4 ratio, and the observed reaction orders greater than 1 [57]. The formed surface oxide structures have been argued as a (111) layer of bulk Ag_2O [58], an Ag_2O-like oxide overlayer with a stoichiometry of $Ag_{11}O_6$ phase [59], or an Ag_9O_6 overlayer [6]. The latest experimental results and first-principle calculations demonstrate that the structures are composed of Ag_6 motifs, such as $P(4 \times 4)$ and $C(3 \times 5\sqrt{3})$ phases, while the latter is exceedingly similar to the former [61, 62]. As a more simple structure, $P(4 \times 4)$ structure consists of two Ag_6 triangles and six O atoms located in the "trough" between Ag_6 triangles. The Ag overlayer with 12 atoms are located approximately above the three-fold sites of the underlying Ag(111) substrate, where half of them are near hcp sites and the others are near fcc sites [61, 62]. It is suggested that the molecular oxygen is active because experiments show that the atomic oxygen in UHV could not be the active oxygen species [63]. For this reason, the mechanism was largely abandoned, but recently it is demonstrated by a combined experimental surface science and DFT approach that oxametallacycles are likely common intermediates in both epoxidation and combustion [13, 14, 48]. A microkinetic model for ethylene epoxidation is successfully established based on a reaction coordinate calculated from first principles incorporating the oxametallacycle as a central intermediate [15]. A similar reaction coordinate has been calculated [16] for both metallic silver and a surface silver oxide [47, 56].

(1) Ethylene epoxidation on Ag(111)

On Ag(111), it has been suggested that the surface-mediated addition of ethylene to oxygen is the rate-determining step. Generally, the atomic adsorbed oxygen is accepted as the active species in the epoxidation of ethylene. Thus, the first step of the ethylene epoxidation is the dissociation of molecular oxygen. In Fig. 1, the calculated reaction coordinate for ethylene epoxide on silver is shown, where dissociative adsorption of molecular oxygen forms two oxygen atoms, that is, $O_2+2^* \rightarrow 2O^*$. The surface reactions of adsorbed oxygen and weakly adsorbed ethylene to form ethylene oxide via a surface oxametallacycle intermediate, $C_2H_4^*+O^* \rightarrow C_2H_4O$. The dissociation of oxygen on silver is activated, with activation energies of ∼1.61 eV on Ag(111) and ∼0.75 or 0.26 eV on step sites depending on the function used. Thus, it should take place mostly on stepped sites, which is the first step in Fig. 1. The enthalpy of reaction for oxygen dissociation on Ag(111) is estimated to be about –0.35 eV for a Ag(111) terrace and about –0.65 eV for a Ag step. As ethylene approaches the oxygen-covered sites on the Ag surface, the interaction between ethylene carbon atoms and oxygen adatoms takes place. This interaction results in the formation of TS_1 as shown in Fig. 1. It is observed that the C–C bond is elongated from 1.33 Å for the gas-phase ethylene to 1.38 Å for the TS, consistent with the expected decrease of the C–C bond order. Also, the C_1–O bond is being formed in the TS as evidenced by the change in the hybridization of the C_1

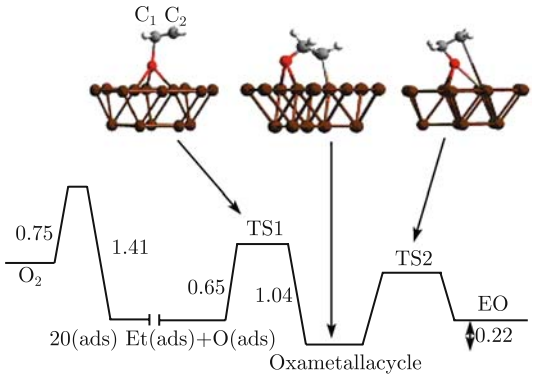

Fig. 1 Calculated reaction coordinate for ethylene epoxidation on silver. Energy units are eV. The discontinuity in the reaction coordinate reflects the change in oxygen molarity. The barrier for oxygen dissociation is from Ref. [65].

carbon from sp^2 to sp^3 with perturbation of the planar configuration corresponding to gas-phase ethylene. The activation energy for this elementary step is found to be 0.65 eV as calculated by cluster and periodic DFT calculations, accounting for 0.35 eV for the heat of ethylene adsorption. The product of this elementary step is the oxametallacycle. This surface intermediate is similar to the surface intermediate that is spectroscopically identified during the dissociative adsorption of ethylene oxide on Ag(111) [64].

The next step is the formation of ethylene oxide from the surface intermediate. Extensive DFT calculations show that the formation of ethylene oxide from the surface intermediate in Fig. 1 involves two characteristic motions. The first is the motion of the weakly bound carbon, C_2, away from the Ag surface. The approach of C_2 and the oxygen atom leads through TS_2 to the formation of ethylene oxide. Careful examination of TS_2 clearly suggests the formation of a ring structure. The C_2–O bond is beginning to form and the O–Ag bonds are elongated as well, suggesting that the product of this elementary step is the gas-phase ethylene oxide, which was confirmed by the calculations.

It is concluded that ethylene reacts with adsorbed oxygen to form a surface intermediate previously identified as a surface oxametallacycle [64]. This intermediate reacts to form the gas-phase ethylene oxide. A possible reason for the unique ability of silver to selectively catalyze ethylene epoxidation stems from the fact that silver provides a binding environment. The environment is strong enough to dissociate oxygen but weak enough to allow facile surface reaction and desorption of ethylene oxide.

(2) Ethylene epoxidation on $Ag_{12}O_6$/structure

At O_{down}–Ag_1 site shown in Fig. 2(A), C_2H_4 plus $Ag_{12}O_6$ structure is taken as the initial state. C_2H_4 is adsorbed weakly at Ag_1 site as discussed above ($E_{C_2H_4}$ = 0.119 eV). The E_a to produce a five-membered ring containing a backbone O–C–C linkage and two Ag atoms (OMME) from the C_2H_4 adsorbed state is 0.23 eV, which is between E_a = 0.32 eV on O/Ag(111) [17] and E_a = 0.17 eV on $O/Ag_{cluster}$ structure [13]. At the TS_1, the energetic level is 0.11 eV larger than that of the initial state where a C–O bond is created through a lateral shift of C_2H_4 toward O_{down}. Meanwhile, O_{down} moves upward. Let subscript denote the corresponding bond, l_{C-C} of C_2H_4 at TS_1 shown in Fig. 2(A)c is elongated from 1.330 to 1.377 Å, which is consistent with that of 1.38 Å on $O/Ag_{cluster}$ structure [13]. After TS_1 state is reached, OMME is built with energetic drop of 0.05 eV from the initial state. In the next step, C_2H_4O is formed from OMME via the TS_2 with E_a = 0.15 eV, which is smaller than the experimental and simulated values of E_a = 0.20 eV [16], E_a = 0.92 eV adsorbed on O/Ag(111) [17], and E_a = 0.18 eV adsorbed on $O/Ag_{cluster}$ structure [13]. In Fig. 2(A)e, C_2 moves away from Ag_1 toward O_{down} atom and C_2–O_{down} bond begins to form with $l_{C_2-O_{down}}$ = 2.155 Å. Compared with OMME, the $l_{C_2-Ag_1}$ bond at TS_2 state is elongated from 2.286 to 3.439 Å, while the l_{C-C} bond is shortened from 1.509 to 1.460 Å. Thus, the product of this elementary step is C_2H_4O [13]. The energetic level at TS_2 is 0.10 eV higher than that of the initial state. Thus, combination of C_2H_4O and the oxygen-deficient oxide $Ag_{12}O_5$ is weak and has only a size of 0.06 eV. The C_2H_4O+$Ag_{12}O_5$ as the product of C_2H_4+$Ag_{12}O_6$ is 0.02 eV more stable than C_2H_4+$Ag_{12}O_6$. Considering experimental E_a values with a broad range of 0.2 to 1.1 eV [16, 17], this process could be realized. Note that the extraction of an O from $Ag_{12}O_6$ makes little reconstruction of the surface oxide. To complete this catalytic cycle, E_a for O_2 dissociation on $Ag_{12}O_5$ examined is 0.63 eV, which agrees with E_a = 0.64 eV on O/Ag(111) [17]. At the O_{up}–Ag_2 site, the reaction process of C_2H_4 is analogical with that at O_{down}–Ag_1 site as shown in Fig. 2(B).

At two sites in Fig. 2, the ethylene epoxidation mechanisms are reasonably semblable in terms of both structures and energies. The initial state for both possible

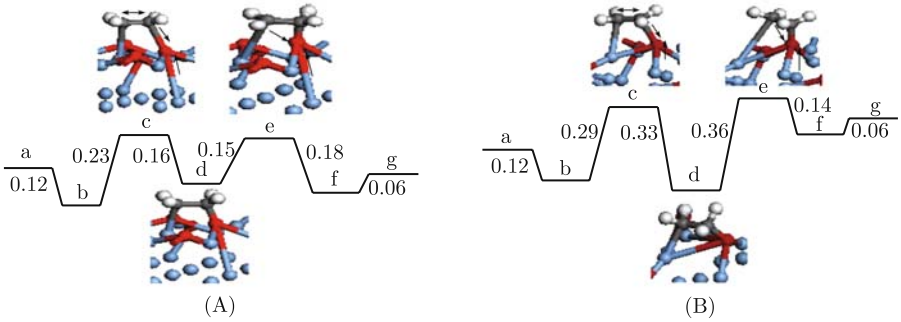

Fig. 2 Relative energy diagram for the conversion of C_2H_4 to C_2H_4O at O_{down}–Ag_1 **(A)** and O_{up}–Ag_2 sites **(B)** on $Ag_{12}O_6$/Ag(111) overlayer using LST/QST tools. The panels from a to g indicate the corresponding states, which are, in turn, the gas-phase C_2H_4 and $Ag_{12}O_6$ structure, C_2H_4/$Ag_{12}O_6$ structure, TS_1 and $Ag_{12}O_6$ structure, OMME/$Ag_{12}O_5$ structure, TS_2 and $Ag_{12}O_5$ structure, C_2H_4O/$Ag_{12}O_5$ structure, and gas-phase C_2H_4O and $Ag_{12}O_5$ structure. The structures shown correspond to TSs and OMME where the arrows depict the motion of atoms during the reaction. The numbers shown denote the energetic change values E_a in eV between adjacent two states. Reprinted in part with permission from Ref. [14]. Copyright © 2007 American Chemical Society.

processes is identical. The two TSs with larger E_a values at the O_{up}–Ag_2 site, however, are much harder to reach, while OMME at O_{up}–Ag_2 site is more stable than that at O_{down}–Ag_1 site. It is known that a good catalyst is characterized by low activation energy and weak bonding of the intermediates [65]. For the intermediate in Fig. 2, at O_{down}–Ag_1 site, $E_a = 0.16$ eV to reform the adsorbed C_2H_4, which is larger than that to form C_2H_4O ($E_a = 0.15$ eV). The corresponding values at the O_{up}–Ag_2 site are 0.33 and 0.36 eV, respectively. This energetic difference brings out the preferred O_{down}–Ag_1 site for the ethylene epoxidation in comparison with the O_{up}–Ag_2 site. Moreover, the whole reaction of C_2H_4O at the O_{down}–Ag_1 site is degressive in energy, being opposite to that at the O_{up}–Ag_2 site. Also, the energetic difference at the two sites after the process is 0.14 eV, which is consistent with the difference of $E_{r,up}$–$E_{r,down} = 0.13$ eV as shown above. However, O_{up} is easier to recover for its lower O_2 dissociation barrier, which leads to larger recovering rate and is beneficial to the process. Thus, in reality, both sites should contribute to the ethylene epoxidation process, while the other two sites are impossible.

Obviously, ethylene can easily react with the oxygen of Ag surface oxide (Ag_6O_6) to form a surface intermediate and then to the ethylene oxide. Moreover, the Ag_6O_5/Ag(111) structure can easily release the ethylene epoxidation and react with oxygen to the Ag_6O_6/Ag(111) one.

3.1.2 Benzene dehydrogenation

The catalytic conversion of aromatic molecules on transition metal surfaces and their dehydrogenation or hydrogenation reaction are very important in the chemical industry and science for both environmental and economical reasons [66–68]. Furthermore, the adsorption of organic molecules on transition metal surfaces is of great relevance to a wide range of systems, from the tuning of self-assembled monolayers to heterogeneous catalysis [11]. In addition, open-shell organic molecules have been the subjects of considerable interest for over 100 years. Especially, the properties of organic radicals have been intensively studied, including thermochemical stabilities, chemical reactivities, and molecular and electronic structures [69].

The interaction between aromatic compounds and various substrates has been and continues to be one of the hot fields in surface science since 1970s. As the simplest aromatic molecule, the adsorption behavior of benzene has received much attention. The electronic and geometric structures, work function, and vibrational properties of adsorbate/substrate systems have been studied by various techniques on different surfaces, Co(1010) [70], Pt(111) [71, 72], Pd(111) [73], Rh(111) [74], Cu(100) [75], Cu(110) [76], Cu 111) [77, 78], Ag [79–81], Au(111) [82], and Au [83].

On the Cu(111) and Cu(100) surfaces, it is generally concluded that benzene adsorbs with the aromatic ring parallel to the surface. This adsorption geometry suggests that the out-of-plane benzene p orbitals are mainly involved in the bonding process. Benzene chemisorption on transition metals has also been studied as a model system for unsaturated hydrocarbon catalysis [84]. An example is the catalytic coupling of propyne on Cu(111), yielding benzene among other products [85]. In relation to the pure benzene, copper is quite inert [85–88], and some theoretical works [89] concluded that the interaction is so small that benzene physisorbs on Cu(100).

The manipulation of benzene molecules on Cu(100) with the scanning tunneling microscope (STM) leads to the dissociation of benzene into smaller fragments [90, 91]. The interpretation given is that benzene undergoes a dehydrogenation reaction caused by the tunneling current, which is also analyzed by DFT calculations [11]. The symmetry and corrugation of the constant current STM images of the remaining fragments have been interpreted to indicate that benzene is produced. Thus, the removal of two hydrogen atoms from the benzene molecule appears to be more favorable than the removal of a single hydrogen. However, singly dehydrogenated fragments are perfectly stable on noble metal surfaces. Phenyl fragments are found after iodobenzene dissociation on Cu(111) [92]. Phenyl has been extensively studied on Cu surfaces [93].

For the catalyst used for the conversion of aromatic molecules, Pt is one of the most important catalysts where benzene experimentally was adsorbed parallel to the Pt surface in UHV [94–96] under electrochemical conditions [97]. For the adsorption of benzene on Pt surface, it is now clearly established that, at low coverage, the bonding of benzene is exclusively through the π electron system, resulting in a parallel or flat configuration on the close-packed transition metal surfaces. This is also proven by the DFT calculations, which show both bri30° and hcp0° being adsorbed sites, where hcp and bri, respectively, denote the hollow and bridge adsorbed sites, while 0° and 30° denote the angles of C–C bonds being rotated with respect to the atomic directions on the surface. Meanwhile, the ring distortion has been observed to eliminate ring tension as a result of the interaction of the benzene ring π electron cloud with the surface [67, 68, 71, 72, 98]. For small Pt cluster models [99–101], benzene adsorbed on Pt has a staircase structure [100] or a tilted di-π adsorption mode [101].

In the case of benzene dehydrogenation on Pt surface, benzene is dehydrogenated to leave an adlayer of stoichiometry C_6H_3 or C_2H at 420 to 565 K, which is further decomposed to graphitic carbon and hydrogen at 810 K

on Pt(111) surface [102]. For benzene on Pt/ZnO(0001)–O model catalysts, its dehydrogenation probability on 2D Pt islands is higher than on Pt(111) surface and may depend on island dimensions [103]. DFT calculations indicated that the phenyl (C_6H_5) and *ortho*-benzene (*o*–C_6H_4) could be formed in the dehydrogenation of benzene on Pt(111) surface cluster model [67]. Moreover, the decomposition of benzene on Pt surfaces were studied [96, 104, 105]. The C–H bonds are believed to break first on Pt(111) surface and Pt(100) [106]. It is also found that C_6H_3 is an intermediate for decomposition of C_6H_5 on Pt(111) surface [107]. Furthermore, reactive molecules (hydrocarbon fragments) derived from gas-phase benzene are phenyl, benzene, and triadical [69]. DFT calculations also find two minimum energy pathways for the dehydrogenation of benzene on Pt(111), where the adsorption property and electronic structure of the dehydrogenation radicals are also considered.

(1) Benzene dehydrogenation on Cu(100)

In the case of benzene dehydrogenation on Cu(100), the first hydrogen scission leads to a phenyl radical C_6H_5 and the second one results in the benzene species, C_6H_4. As previously found [108], both dehydrogenation products stand upright on the surface at bridge and hollow sites, respectively, for C_6H_5 and C_6H_4, which are shown in panels 2 and 3 of Fig. 3. For the two endothermic steps, each TS is determined by an NEB calculation followed by a thorough vibrational analysis of the TS. The TS geometry and imaginary frequency are provided in the top panel of Fig. 3. The imaginary frequencies correspond to soft modes, revealing the appearance of a saddle point and hence characterizing the TS. In the reactions analyzed here, the reaction coordinates correspond to a stretch mode of a loose C–H bond as marked by dotted lines in the top panel of Fig. 3. Notably, the TS_{1-2} and TS_{2-3} geometries in Fig. 3 exhibit similar atomic positions for the breaking σ bond. The loose C–H bond is actually involved in a three-membered metallacycle Cu–C–H. In other words, C and H atoms share almost the same on the top adsorption site [109], as previously observed for the reverse hydrogenation mechanism [110]. This similarity between the geometrical structures of TS_{1-2} and TS_{2-3} is in apparent contradiction with different activation energies: the first dehydrogenation step costs almost 0.3 eV more than the second step. This energy difference is related to the adsorption energy of the benzene molecule. Indeed, in order to react, the benzene molecule first desorbs and almost aligns its molecular plane with the surface normal while pointing one C–H bond toward one single metal atom. As a result, this transient upright benzene and the phenyl radical react similarly regarding the dehydrogenation reaction: their hydrogen scission intrinsically costs ∼1.5 eV. This quantity agrees with estimates based on the dehydrogenation of benzene on Cu(110) [111]. However, the calculated gas-phase dehydrogenation barrier is 4.5 eV [112]. This large energetic difference between the gas and chemisorbed phases is due to the attractive interaction between the reaction products and the metallic surface. The experiments on STM-induced dehydrogenation find a reaction threshold at 2.9 eV on Cu(100) [113] or 2.4 eV on Cu(110) [111], the difference probably stemming from the measuring method rather than from physical properties [111]. At 1.5 eV, the molecule would hop away from its original site, but no C–H fragmentation could be observed [113]. These data are in good agreement with the adiabatic barriers of Fig. 2 because breaking the C–H bond globally costs 1.85 eV, but the molecule can already desorb at 1.5 eV. The threshold to the TS_{1-2} state is well below the experimental 2.4 eV needed to dehydrogenate the molecules. Hence, at 1.5 eV, the only possible reaction is desorption, while at 2.4 eV dehydrogenation is possible. As discussed in Ref. [111], our calculations confirm that the 2.4 eV onset is not connected with the activation barrier for the C–H bond breaking. The minimum energy required to traverse both TS_{1-2} and TS_{2-3} in a single step is 2.32 eV. However, if the crossing of the first TS dissipates all of its minimum ex-

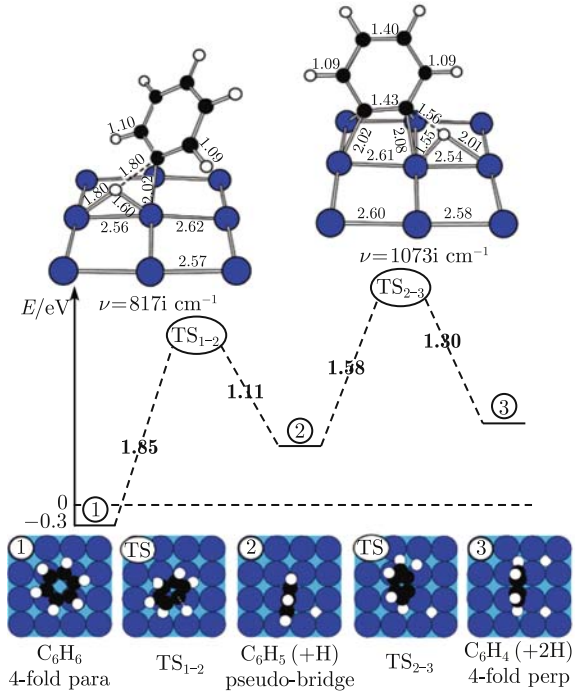

Fig. 3 Energy profile for the successive dehydrogenation of C_6H_6 on Cu(100) with respect to the sum of energies of the free benzene molecule and the relaxed Cu(100) surface. The geometrical structures of the TSs are given in the top panel with bonding distances in Å and with the imaginary frequency of the soft mode at the reaction coordinate, which corresponds to a weakening C–H stretch mode (*dotted line*). Top views of all states along the reactive profile are given in the lower panels with the symmetry of their adsorption site. Reprinted in part with permission from Ref. [11]. Copyright © 2007 American Chemical Society.

cess energy through the recoil of its departing hydrogen atom, an additional 1.11 eV of energy, making 3.43 eV in total, would be required. Hence, detailed knowledge of the reaction dynamics must be obtained before accurate estimates of the actual threshold energy can be made.

(2) Benzene dehydrogenation on Pt(111)

As shown in Fig. 4, benzene dehydrogenations at both bri30° and hcp0° sites lead to formation of 2a-dehydrobenzene [69, 114, 115]. The minimum energy required to traverse the three TSs in a single step is 3.21 eV at bri30° site compared with 3.06 eV at hcp0° site. Thus, both minimum energy pathways may be feasible. Considering their comparability, we take those at hcp0° site as examples.

At the hcp0° adsorbed site, the dehydrogenation of benzene brings out 2a-dehydrobenzene (2a–C_6H_3) as shown in Fig. 4(A). For the first C–H scission, the calculated energetic values are $E_{a,1} = 1.65$ eV and $E_{r,1} = 0.50$ eV. In experiments, the barrier for benzene dehydrogenation is found to be 1.21 to 1.87 eV [102, 116, 117]. On a cluster model, E_r for the dehydrogenation of hollow-bound benzene is endothermic by 0.52 eV [67]. C_6H_5 is adsorbed through C at the top site on Pt(111) surface with the adsorption energy $E_{ad} = 2.78$ eV. Its C ring plane is tilted to the surface with a straight z-axis on Pt(111) surface as shown in Fig. 4(A)c. The intermediate phenyl C_6H_5 is further dehydrogenized to *ortho*–benzene (o–C_6H_4). The calculated energetic values are $E_{a,2} = 1.39$ eV and $E_{r,2} = 0.01$ eV. o–C_6H_4 is perpendicularly adsorbed at bridge site with $E_{ad} = 4.09$ eV. The same adsorbed site for o–C_6H_4 is found on a Pt cluster with $E_{ad} = 3.88$ eV [67]. For the first and second C-H scissions, the geometry structures of $TS_{b,1}$ is close to that of $TS_{d,1}$ for the breaking of σ bond as shown in Fig. 4(A). Moreover, the loose C–H bonds for these two TSs are all involved in a three-membered metallacycle Pt–C–H. Thus, the benzene molecule may firstly be desorbed and it almost aligns its molecular plane with the normal while pointing one C–H bond toward one single metal atom for dehydrogenation. This mechanics is proven on Cu(100) [11]. The third C–H bond scission produces dehydrobenzene 2a–C_6H_3. $E_{a,3}$ and $E_{r,3}$ are 2.53 and 1.12 eV, respectively. $E_{a,3} > E_{a,2}$. The reason could be that the dehydrogenation mechanics in the third step differs from that in the former two steps. The calculated 2a–C_6H_3 is slightly tilted adsorbed on Pt(111) surface through four C–Pt bonds with $E_{ad} = 5.10$ eV. The distance of C_1 and C_3 in the adsorbed 2a–C_6H_3 is 2.50 Å. This distance is proposed to be 2.37 Å for the $^2B_2$ state of gas-phase 2a–C_6H_3, where $^2B_2$ denotes that there is no bond forming between C_1 and C_3 atoms as shown in Fig. 4(A)g [114, 115]. Thus, the calculated 2a–C_6H_3 should also have a $^2B_2$ state as predicted in a computational study for the gas-phase 2a–C_6H_3 [118]. The IR spectroscopic data indicated the presence of a $^2A_2$ with a relatively short C_1–C_3 distance of 1.69 Å, where $^2A_2$ shows the formation of C_1–C_3 bonding [114, 115]. This state is a slightly preferred one compared with the $^2B_2$ one [114, 115]. The preference of $^2B_2$ state for adsorbed 2a–C_6H_3 is due to the attractive interaction between 2a–C_6H_3 and the metallic surface.

Figure 5 presents the electron density or the electron transfer during the above dehydrogenation process. Moreover, the 2-D slices of the electron density difference are shown in Fig. 5(B). The denser the color is, the more the electron density changes. It is known that the predominant effect of the above electron transfer is the interaction between the aromatic π states and the d band of the Pt(111) surface. This case is shown in Fig. 5(A)a and c. The donation of electrons from C_6H_6 to Pt and the back-donation are nearly in balance (the back-donation is slightly larger). There is a little difference between C_6H_6 adsorbed at bri30° and hcp0° sites. Some electrons are accumulated between C_1 and Pt atom at

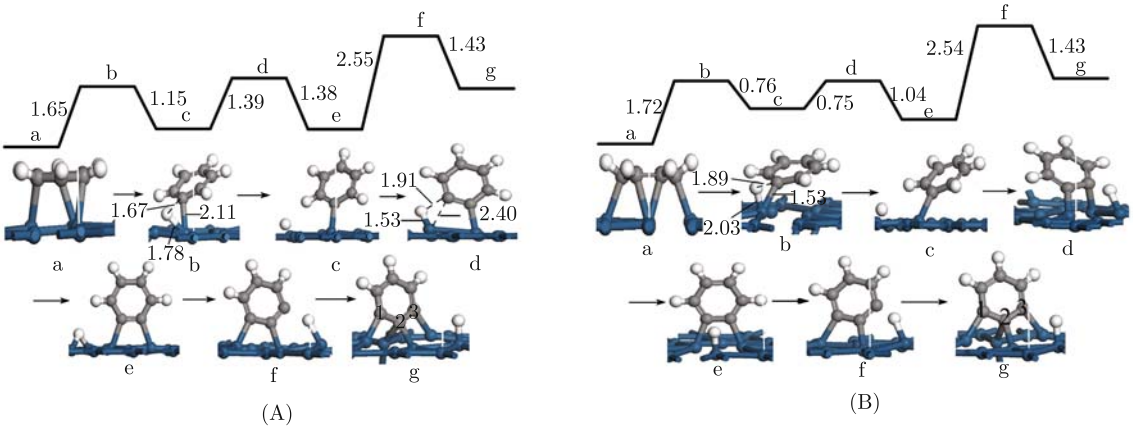

Fig. 4 Two minimum energy pathways for the dehydrogenation of benzene on Pt(111) surface. **(A)** indicates the reaction coordinate for the dehydrogenation of benzene at hcp0° site, while **(B)** indicates that at bri30° site. a, c, e, and g present the intermediates, while b, d, and f present the TS. The energies between two states are shown in eV. Three-membered metallacycle Pt–C–H in $TS_{b,1}$, $TS_{d,1}$, and $TS_{b,2}$ are marked by short dot lines and the distance of atoms are also shown in Å. Reproduced with permission from Ref. [12].

bri30° site as shown in Fig. 5(A)c. As reported in literature [66], C_1 atom is σ bonded to Pt atom at bri30° site, except the interaction between the aromatic π states and the d band of the surface, which could be observed more clearly from the 2D slice of electron density difference.

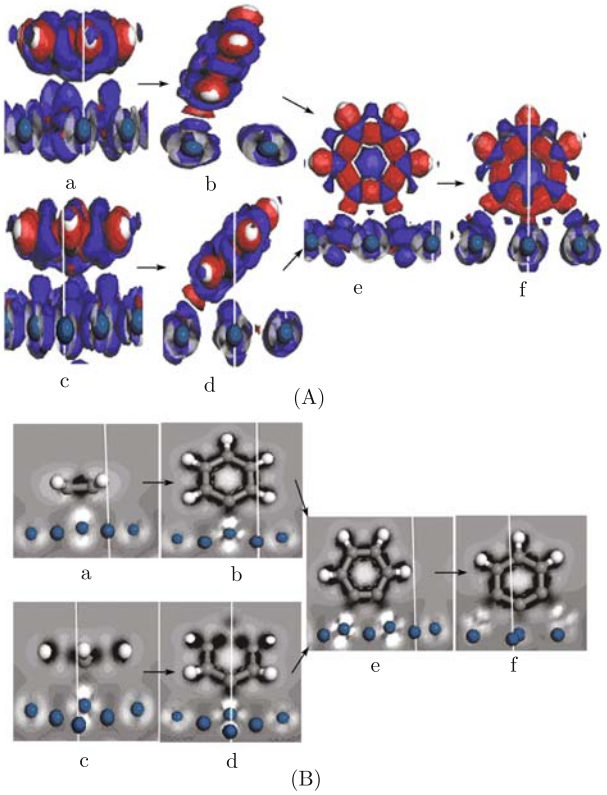

Fig. 5 The plots of the electron density difference. In **(A)**, the order of a→b→e→f is accorded with the dehydrogenation of benzene at hcp0° site, while the order of c→d→e→f is accorded with that at bri30° site. The red (*black*) region shows the electron accumulation, while blue (*gray*) region shows the electron loss. In **(B)**, the 2-D slice of electron density difference as shown in **(A)** is present. b and d are the different elevations of **(A)**b and d. The black region shows the electron accumulation, while white region shows the electron loss. Reproduced with permission from Ref. [12]. Copyright © 2008 American Institute of Physics.

For C_6H_5 produced at bri30° site in Fig. 5(B)d, C_1 gets more electrons from Pt atom, forming an σ-like bonding. The enhancement of C_1/substrate interaction leads to an important rehybridization with metallic states. Meanwhile, the bond length of C_1–Pt bond decreases from 2.19 Å in Fig. 5(B)c to 2.01 Å in Fig. 5(B)d. It can be seen in Fig. 5(A)d that the d bands of Pt atoms at the bridge site also interact with the aromatic π states. For C_6H_5 formed at hcp0° site, electrons are accumulated between C and Pt atoms, which are similar to that at bri30° site in Fig. 5(B)b. The σ-like bonding and C–Pt bond length are the same as that formed at bri30° site. The interaction between the d band of Pt atoms and the aromatic π states, however, nearly disappears as shown in Fig. 5(A)b. It is known that, in a C_6H_5/Cu(100) system, the σ bonding interaction tends to cause the C ring to stand perpendicular to the surface, while the π bonding tries to optimize the overlap with the substrate, pushing the C ring parallel to surface [119]. Thus, the C ring of C_6H_5 adsorbed on Pt(111) surface is also tilted in our case. Moreover, θ is changed from 56.6° at bri30° to 69.4° at hcp0°, when the interaction between the d band of Pt atoms and the aromatic π states is weakened.

For the C_6H_4 adsorbed on Pt(111) surface shown in Fig. 5(B)e, electrons are also accumulated between C and Pt atoms with two σ-like C–Pt bonds where $L_{C_1-Pt} = L_{C_2-Pt} = 2.00$ Å. Although the intensity of orbital hybridization between C_1 and Pt atom in Fig. 5(B)d and e cannot be determined, increased bond numbers certainly increase the electron accumulation between C and Pt atoms and strengthen the σ-like bonding. This leads to the perpendicular adsorbed geometry of C_6H_4 as that on Cu(100). Accordingly, no interaction between the aromatic π states with the d band of Pt atoms is detected in Fig. 5(A)e.

The adsorbed property of C_6H_3 has not been reported before, which is present in Fig. 5(B)f. Note that only two C–Pt bonds of 2-D slice can be observed in Fig. 5(B)f due to the complicity of the four bonds. Indeed, it can be seen in Fig. 5(B)f that the property of these four C–Pt bonds are similar to those in Fig. 5(B)d and e. Its adsorbed structure agrees with the former benzene radicals where $L_{C_1-Pt} = L_{C_2-Pt1} = L_{C_3-Pt} = 2.02$ Å and $L_{C_2-Pt2} = 2.14$ Å. As discussed above, these four C–Pt bonds should be the σ-like bonding. The larger size of L_{C_2-Pt2} may result in a slightly tilted C_6H_3 adsorbed geometry.

3.1.3 C_2H_2 adsorbed on Cu surface

Organic molecular adsorption on metallic surfaces is a critical phenomenon in heterogeneous catalysis, tribology, electrochemistry, and material processing [120]. The adsorption system of acetylene (C_2H_2) on Cu surfaces has initiated a lot of scientific interest, as it involves notable elementary catalytic reactions, such as the trimerization reaction of C_2H_2 to form benzene on Cu substrates [121, 122]. In general, C_2H_2 always decomposes on transition metal surfaces (such as Pd, Pt, Ni, and Rh) at low temperature, and the adsorption behaviors of C_2H_2 on these surfaces are different [123]. In particular, the trimerization reaction of C_2H_2/Cu is unique due to the formation of complex molecules on the metal surfaces [124]. Recent research has demonstrated that Cu is a much more versatile C_2H_2coupling catalyst than Pd. This is because C_2H_2 trimerization on Cu surface is far less structure-sensitive than on the Pd surface, and the adsorbate mobility is also higher [122]. In addition, unlike ethylene (C_2H_4) and ethane (C_2H_6) molecules, the adsorbed C_2H_2 molecule rearranges its geometry and

changes its intramolecular binding significantly, which provides insight into the fundamental chemistry of triple C–C bonds on the metallic surfaces [125, 126].

For the C_2H_2/Cu(100) system, C_2H_2 molecules lie on substrates as determined by the near-edge X-ray absorption fine structure (NEXAFS) but did not give definitive adsorption sites and orientations [127]. Subsequently, it is analyzed the NEXAFS spectra by the multiple scattering cluster (MSC) method that C_2H_2 molecules adsorb on the "two-fold aligned bridge" site of Cu(100) surface [128]. However, observation with STM and inelastic tunneling spectroscopy (IETS) is against the aforementioned results [129, 130]. It exhibits that the "four-fold diagonal hollow" should be the most preferable site, i.e., C_2H_2 adsorbs on the hollow site of Cu(100) surface, with the plane of the molecule across the diagonal of the four Cu atoms with square configuration [121]. This has been verified through the determination of charge transfer from Cu to C_2H_2 [131].

For C_2H_2/Cu(111) system, it is suggested that C–C axis parallels to Cu(111) surface over a bridge site, but no information about H was given from photoelectron diffraction [132]. It also reported the temperature-programmed reaction of C_2H_2 coupling on the Cu(111) surface and observed not only benzene formation but also the formation of butadiene and cyclooctatetraene [122]. Besides C_2H_2/Cu(100) and C_2H_2/Cu(111) systems, the C_2H_2/Cu(110) system has also been investigated [133], where the C_2H_2 adsorption and desorption occurred over a wide temperature range from 280 to 375 K. The adsorption and reactivity of C_2H_2/Cu(110) system are studied using high-resolution electron energy loss spectroscopy (EEL) and thermal desorption spectroscopy [134]. The chemical bonding and geometric structure of C_2H_2/Cu(110) system are analyzed using X-ray photoelectron spectroscopy (XPS), X-ray absorption spectroscopy (XAS), and X-ray emission spectroscopy (XES) [135].

The inelastic scanning tunneling image of C_2H_2/Cu(100) system obtained using a Green function linear combination of atomic orbitals (LCAO) technique is in good agreement with experimental results [126]. The binding energies, geometries, and vibrational frequencies of this system are calculated using LCAO method with cluster models [136]. In the C_2H_2/Cu(100) system, five possible adsorption sites were proposed with the optimized geometry and energy [125]. Subsequently, a "four-fold aligned hollow" was suggested as the preferable adsorption site. This may be a result of problems involving the cluster modeling of metal surfaces [125]. Theoretical and experimental studies of chemisorption parameters and STM images for C_2H_2/Cu(100) system are reported [137, 138], where the geometric and electronic structure and vibrational energies were obtained from DFT calculations. For the C_2H_2/Cu(111) system, a cluster model with only four Cu atoms, with one located in the first layer and the other three in the second layer, is studied [139]. The cluster models with more complex geometry variations are also developed [140]. For the periodic boundary conditions, the C_2H_2/Cu systems are systematically studied, where the most stable adsorption sites, the orientations of C_2H_2 molecules and Cu substrates, the related geometric parameters, and the charge transfer information are also achieved [141].

(1) C_2H_2 adsorbed on Cu clusters

The adsorption site and orientation of C_2H_2 on Cu(001) have been determined unambiguously by STM: the molecule is adsorbed on the hollow sites, with the plane of the molecule across the diagonal of the square formed by 4 Cu atoms and the C–H bonds tilting away from the surface [142, 143]. This orientation is related to the excited state of acetylene in gas phase [144]. The cluster model constructed consists of C_2H_2 and 21 Cu atoms [Fig. 6(a)]. $E_{ad} = -2.70$ eV by LDA and –1.09 eV by GGA. The optimized tilting angle of the C–H bonds to the surface and the lengthening of the C–C bond are in good agreement with near-edge X-ray adsorption fine structure data [145, 146] and previous calculations [147]. The vibrational frequencies of C_2H_2/Cu(001) are calculated in the harmonic approximation, assuming the displacement fields to be strictly localized to an H(D) atom

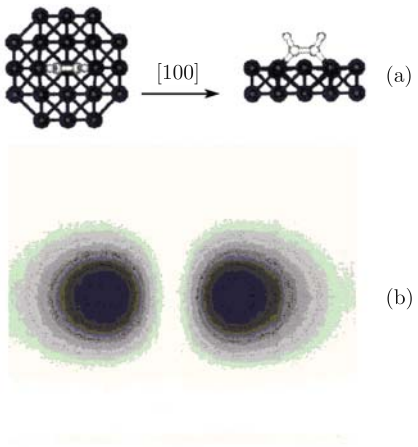

Fig. 6 The adsorbed structure and STM image of C_2H_2/Cu(100). In **(a)**, top view (*left*) and side view (*right*) of the cluster are shown, while the STM image is shown in **(b)**.

Table 1 Experimental and calculated vibrational frequencies of C_2H_2 on Cu(001). The calculated frequencies of Ref. [147] are shown in the parentheses.

Mode	Experimental	Calculated	Error
ν(CH)C_2H_2	358	364	6, 7
ν(CC)C_2H_2	164	176	12
δ_{as}(CH)C_2H_2	141	134	–7
δ_s(CH)C_2H_2	118	119	1
γ(CH)C_2H_2	78	87	9
ν(CM)C_2H_2	52	60	8

Table 2 Comparison of our calculated adsorption energy E_{ad} and interaction energies E_{int} values in eV/molecule on all the possible adsorption configurations. Reprinted in part with permission from Ref. [141]. Copyright © 2007 American Chemical Society.

	C_2H_2/Cu(100)					C_2H_2/Cu(111)				
Type	I	II	III	IV	V	I	II	III	IV	V
$-E_{ad}$	0.48	(1.38)[a]	(1.38)	1.22	1.38	0.45	(1.17)	(1.17)	(1.17)	1.17
$-E_{int}$	2.32	(4.08)	(4.08)	3.88	4.08	2.69	(3.95)	(3.95)	(3.95)	3.95
	C_2H_2/Cu(110)-long[b]					C_2H_2/Cu(110)-short[b]				
Type	I	II	III	IV	V	I	II	III	IV	V
$-E_{ad}$	(1.13)	0.56	0.99	1.13	(1.13)	0.55	0.81	0.99	0.67	(1.13)
$-E_{int}$	(4.17)	1.71	3.97	4.17	(4.17)	2.11	3.79	3.97	3.60	(4.17)

[a] The parentheses indicate that the configurations are unstable, and convert to the most stable ones spontaneously after full relaxation. Thus, their E_{ad} values are the same as those of the most stable ones.
[b] C_2H_2 may adsorb along the [001] and [110] directions of Cu(110), since the unit cell of the (110) surface is a rectangle.

for the C–H(C–D) modes and to keep the other bonds rigid [147]. Their results are displayed in the parentheses of Table 1. It can be seen that there is satisfactory agreement between the experimental and the calculated vibrational frequencies, especially for the C–H stretch modes, which can be a benchmark of the further calculations. For STM images, note that in the experimental images of C_2H_2 (C_2D_2) on Cu(001) the positions of the hydrogen (deuterium) atoms appear somewhat bright [143]. One can see from Fig. 6(b) that the simulated image reproduces this feature well. As stated above, the binding energies, geometries, STM images, and vibrational frequencies for the C_2H_2 on Cu(001) obtained using cluster model agree well with the available experimental results.

(2) C_2H_2 adsorbed on Cu surface

For the periodical system, C_2H_2 molecule is adsorbed on one surface of the Cu slabs, where a uniform (2×2) unit cell is set with a C_2H_2 coverage of 0.25 monolayer (ML) [141]. There are five possible adsorption configurations, namely "two-fold aligned bridge" (Type I), "two-fold perpendicular bridge" (Type II), "three-fold hollow" (Type III), "four-fold aligned hollow" (Type IV), and "four-fold diagonal hollow" (Type V) [125, 128]. The calculated E_{ad} and E_{int} values are listed in Table 2. For the C_2H_2/Cu(100) system, if type V is used as a reference, the E_{ad} values of types I and IV are 0.90 and 0.16 eV larger, respectively. It is of interest to note that type V was converted from initial configurations of types II and III spontaneously once the full relaxation took place. Therefore, type V is the most stable adsorption site for C_2H_2/Cu(100), which corresponds to experimental observations [121, 129, 130]. However, if the cluster model with 12 Cu atoms in the first layer and 5 Cu atoms in the second layer is employed, the calculated E_{ad} values have the order II>I>III>V>IV, which differs from experimental results. For the C_2H_2/Cu(111) system, $E_{ad,I} = -0.45$ eV is 61.54% greater than $E_{ad,V} = -1.17$ eV, while the other three types convert to type V after the full relaxation. Therefore, type V is also the most preferable site for C_2H_2/Cu(111) system, which corresponds to the experimental observations from the EEL [134] and NEXAFS [148] as well as STM and IETS [132]. Different from the (100) and (111) surfaces, the unit cell of the Cu(110) surface is a rectangle. Thus, C_2H_2 may lie along the [001] (long) or [110] (short) direction of Cu(110) surface. Compared with the data of E_{ad} listed in Table 2, type IV is the preferred adsorption site. Since Cu(110) is the most active surface among the three surfaces [149], the geometry of C_2H_2 adsorption should be very interesting.

As shown in Fig. 7, the blue areas show where the electron density has been enriched, while the yellow ones show where the density has been depleted. Obviously, the C_2H_2 molecules gain electrons, while Cu substrates lose electrons. A similar result of charge transfer has been reported for the saturated hydrocarbons on Cu surface [150]. In Fig. 7(a), the orbitals of C_2H_2, which lie on the Cu(100) substrate, lead to a larger E_{int} value. From Fig. 7(b), it is discernible that the orbital hybridization between C_2H_2 and Cu is much weaker than that of Fig. 7(a), showing a weaker binding strength of C_2H_2/Cu(111). The orbital hybridization between the adsorbate and the Cu(110) surface is the largest among the three surfaces: as shown in Fig. 7(c), the blue and yellow areas are strongly mixed. Some small yellow areas also appear around the C atoms. This is because the charges donated from Cu are not fully accumulated around the C atoms but partially further transferred to H (even make the H tilt) [139, 140].

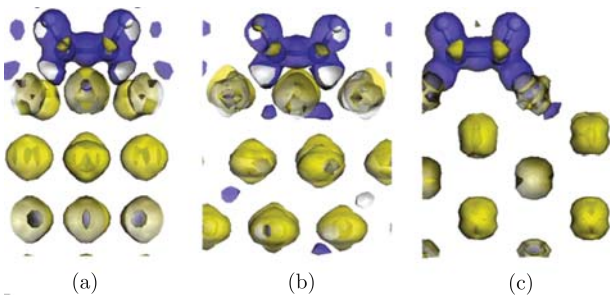

Fig. 7 The plots of the electron density difference: **(a)** C_2H_2/Cu(100), **(b)** C_2H_2/Cu(111), and **(c)** C_2H_2/Cu(110). The blue region shows the electron accumulation, while yellow region shows the electron loss. Reprinted in part with permission from Ref. [141]. Copyright © 2007 American Chemical Society.

In summary, the "four-fold diagonal hollow" is determined to be the most stable adsorption site for the C_2H_2/Cu(100) and C_2H_2/Cu(111) systems, while the "four-fold aligned hollow" is the most stable site for the C_2H_2/Cu(110) system. The variation of the electron density was caused by the electrons moving from Cu to C_2H_2. This results in the intermolecular charge redistribution between the C and H.

3.2 Fuel cell

Direct oxidation fuel cells (DOFCs) have recently intensively researched, as an alternative to hydrogen fuel cells, mainly due to easier fuel storage and handling. The most considered type of DOFC is direct methanol fuel cell (DMFC). Methanol has better oxidation kinetics on Pt-based catalysts in low temperature range than all other aliphatic alcohols and is also known to oxidize completely to CO_2, which leads to better performance of DMFCs.

As the principal chemical process occurring on the anodes of DMFC, the mechanism of oxidation of methanol on a Pt surface is important [151, 152]. The DMFCs offer the potential for direct conversion of methanol to electricity, with efficiencies that are substantially higher than those obtained in the conventionally combustion-based power generation systems [153]. In order to be economically viable, the performance of DMFCs needs to be improved. Therefore, an understanding of the processes occurring on the real fuel cell catalysts under operating conditions is highly desired. Using the differential electrochemical mass spectrometry at potential $E < 0.45$ V, it is claimed that the oxidation of methanol can only be formed via the CO_{ad} (the subscript *ad* denotes the substance in an adsorbed state) intermediate [154]. Analyzing oxidation currents and CO coverage, the methanol oxidation can occur without formation of CO_{ad} at $E > 0.5$ V [155–157]. It is generally accepted that the methanol can be oxidized to CO_2 via a dual-path mechanism [156, 158], that is, via CO_{ad} [159] or non-CO [152] involved reactive intermediates. One of the main issues is whether the CO_{ad} formed during the oxidation of methanol is an intermediate in the serial pathway reaction mechanism or is a byproduct in a parallel reaction mechanism [160].

However, no consensus on the nature of reactive intermediates in the non-CO pathway was given. By using the *in situ* IR reflection-absorption spectroscopy or the surface-enhanced IR absorption spectroscopy with the Kretschmann attenuated total reflectance configuration, various adsorbates, such as formyl $(–HCO)_{ad}$ [161], carboxy $(–COOH)_{ad}$ [161], a dimer of formic acid $(HCOOH)_{2ad}$ [162], and formate $(HCOO–_{ad})$ [152], have been claimed to be the reactive intermediates for methanol electro-oxidation. As an identified intermediate during methanol electro-oxidation, formate was also argued to be a catalyst-poisoning intermediate, like CO_{ad} [163]. For dual pathways of methanol oxidation, it was suggested that the decision between CO and non-CO pathways is made at the initial dehydrogenation step [160, 164]. When $0.2 < E < 0.6$ V, the non-CO pathway was proposed to be essential [162]. When $E \to 0.6$ V, only 75% of the total CO_2 was produced by this pathway [157]. When the Pt(111) surface is modified by cyanide, full oxidation could be realized [165]. Using DFT calculations, the non-CO-involved oxidation of methanol (NCOIOM) pathways on Pt(111) is also systematically researched, which shows that both HCOO– and –COOH are the reactive intermediates with two favored pathways [166].

3.2.1 Competitive paths for methanol decomposition on Pt(111)

It is confirmed that formation of the strong CO_{ad} bonds leads to the self-poisoning of electro-catalysts. The DFT results suggest that three pathways (Fig. 8) may be important in determining the net rate of reaction. The first pathway proceeds as follows: $CH_3OH \to CH_3O \to CH_2O \to HCO \to CO$. This is simply the O–H scission path-

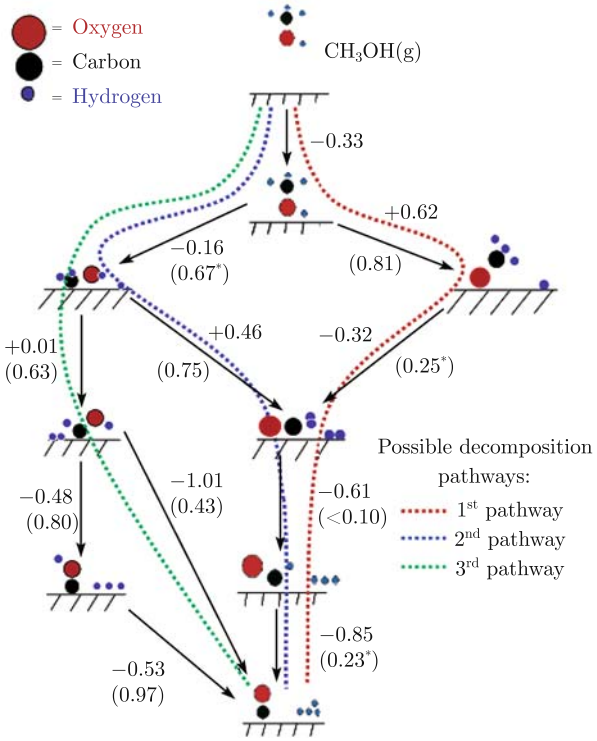

Fig. 8 Schematic summary of the reaction network for methanol decomposition through C–H and O–H bond scission in methanol on Pt(111). Values without parentheses are energy changes of the indicated elementary steps (negative values indicate exothermic steps). Values in parentheses are activation energy barriers. The energies do not include zero-point energy corrections. The dotted lines correspond to likely decomposition pathways for methanol as indicated in the figure legend. Asterisks indicate that such a diffusion barrier (on the order of 0.1 eV) exists for a particular reaction. Reprinted in part with permission from Ref. [153]. Copyright © 2004 American Chemical Society.

way that has already been described in detail [167]; the rate-limiting step of this path way is the first step, the abstraction of hydroxyl hydrogen from methanol. The second pathway involves an initial C–H bond scission in methanol: $CH_3OH \rightarrow CH_2OH \rightarrow CH_2O \rightarrow HCO \rightarrow CO$. According to our results, cleavage of the O-H bond in CH_2OH to produce formaldehyde (CH_2O) would likely be the rate-limiting step of this pathway, although the barrier to C–H bond scission in methanol (the first step in the pathway) is of only slightly lesser magnitude. Note that this pathway was analyzed in a recent publication [168]. The final pathway proceeds as follows: $CH_3OH \rightarrow CH_2OH \rightarrow HCOH \rightarrow CO$. This pathway starts out with C–H scission in methanol. The resulting intermediate undergoes a second C–H scission to produce HCOH. HCOH then decomposes in a quasi-concerted reaction to form CO. This last step begins with O–H scission in HCOH. A configuration resembling adsorbed formyl (HCO) forms, but the C–O bond is tilted at a much higher angle to the surface than is the C–O bond in our previously identified adsorbed formyl species [167]. This pseudo-formyl configuration does not appear to be a stable state. Because of the close proximity of the remaining carbonic hydrogen to the surface, the pseudo-formyl species undergoes spontaneous C–H bond scission to yield CO (we observed this effect with a variety of ionic time steps and different numbers of layers in the platinum slab). This effect appears to be related to the coverage of surface hydrogen; the abstracted hydroxyl hydrogen in HCOH forces the remaining formyl group to rotate away from the abstracted hydrogen. The rotation brings the carbonic hydrogen close to the surface, leading to spontaneous C–H bond scission. The calculations show that the third of these pathways is likely to be dominant under typical reaction conditions.

3.2.2 Pathways for the non-CO-involved oxidation of methanol on Pt(111)

Two pathways are important in determining the net rate of the reaction of the non-CO-involved oxidation of methanol on Pt(111) based on HCOH, which is present in Fig. 9(A). In every step, the energetic changes for adsorption and desorption of molecules are not included due to their low coverage, such as H, OH, and H_2O [164]. Contributions from other co-adsorbed species (such as stable CO_{ad}) are not considered yet herein, since their effects on reactions are expected to be small [164]. The first pathway follows a sequence of HCOH (a) $\rightarrow$ $HC(OH)_2$ (c) $\rightarrow$ HCOOH (e) $\rightarrow$ –COOH (g) $\rightarrow$ CO_2 (I). The rate-limiting step of this pathway is the third step with $E_a = 0.74$ eV, the C–H bond scission in HCOOH. The second pathway has the following reaction way: HCOH (a) $\rightarrow$ $HC(OH)_2$ (c) $\rightarrow$ HCOOH (e′) $\rightarrow$ HCOO– (g′) $\rightarrow$ CO_2 (I′). The rate-limiting step is the fourth step with $E_a = 0.59$ eV. Thus, the second pathway is the kinetically advantaged one and HCOO– should be the active intermediate for NCOIOM. This is consistent with experimental results where HCOO– (bidentate form) was proposed as a reactive intermediate for the non-CO pathway where methanol is oxidized in gas phase either under the atmospheric pressure [170] or in an UHV condition [171] or in the electro-oxidation condition [152]. However, the change of HCOO– from bidentate form to monodentate form costs 0.89 eV. This is close to the barrier energy of C–H scission in HCOOH (0.74 eV). It can be seen in Fig. 9(A) that HCOO– is easier to form and harder to decompose than –COOH. Thus, in reality, both HCOO– and –COOH may be reactive intermediates for NCOIOM. In experiments, it was also suggested that –COOH is a reactive intermediate for non-CO pathway of methanol electro-oxidation [161, 172] in a sequence of $(HCOOH)_{2ad} \rightarrow$ –COOH $\rightarrow$ CO_2 [162]. Moreover, reaction from HCOH to CO_2 is degressive in energy and thermodynamically propitious. These increased stabilities for intermediates would ensure the reaction to proceed certainly, which corresponds to the results on Pt(111) surface [153].

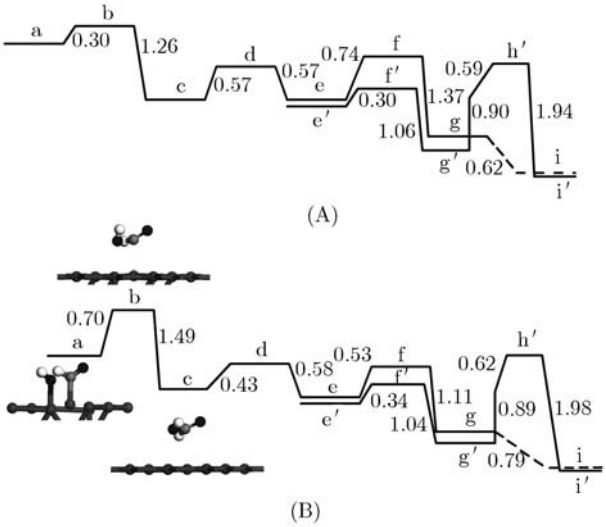

Fig. 9 The relative energetic diagram of two pathways for NCOIOM based on HCOH and –CHO. The dashed line denotes cited values [169]. a, c, e, g, e′, and g′ denote intermediates, while b, d, f, f′, and h′ denote TS. i and i′ denote the products. The substrate is Pt(111), while the gray, red, and white balls in adsorbed molecules denote C, O, and H atoms, respectively.

Figure 9(B)c shows the reaction of OH_{ad} + –CHO $\rightarrow$ HCOOH for NCOIOM pathways based on –CHO where $E_{ad} = 0.70$ and $E_r = -0.79$ eV. Consequently, the intermediate should be HCOOH adsorbed over the top of the Pt(111) surface with $E_{ad} = 1.22$ eV. The distance between C and Pt atom is 2.97 Å. The subsequent reactions are shown in Fig. 9(B), where both HCOO– and –COOH are also reactive intermediates, similar to that in Fig. 9(A). Thus, detailed discussion of these pathways

is ignored.

In conclusion, both HCOO– and –COOH are the reactive intermediates, and reactions via HCOH → $HC(OH)_2$ → HCOOH → HCOO– [–COOH] → CO_2 and CHO → HCOOH → HCOO– [–COOH] → CO_2 are kinetically favored pathways for the non-CO-involved oxidation of methanol. Thus, a non-CO pathway should be entirely feasible in DMFCs.

3.3 Environment

With the increasing level of emissions of pollutants such as NO_x, CO, and hydrocarbons associated to the worldwide expansion of the car market, environmental pollution is getting worse. Thus, the efficient catalysts for cleaning and recycling these wastes are urgently need. More recently, the introduction of catalytic filters for diesel particulate anticipated regulations was used also in advertisements to demonstrate the innovative profile of some car manufacturing companies. Catalysis is thus considered not only as a tool to meet regulations but also part of the factors determining the car appeal to the customers.

It is important to understand the mechanism and catalytic processes of interaction of CO adsorption on metallic surfaces because of their potential use in methanol reforming, fuel cell technology, and, especially, purification of automotive exhaust gases [173, 174]. With the development of calculation ability, many computational studies of CO adsorption on different kinds of surfaces have been reported over the years, especially for surfaces of monometallics [175–179], alloys [180–182], clusters [182–186], and metals supported by oxides [186–188]. The catalytic oxidation on a metallic catalyst surface of 4*d* and 5*d* elements in Group VIII is an efficient way for converting CO to CO_2 at low temperature [189]. In the reaction process of CO/Pt(111) [190], CO/Ru(0001) [191], CO/Rh(111) [192, 193], and CO/Pd(111) [194] systems, the TS and reaction barrier are two crucial requirements [190]. The former determines the amount of products, and the latter decides the catalytic rate. It is known that the amount of CO_2 formation reversely depends on E_{ad} of CO molecules on metallic surfaces [192, 193], which describes the chemical bond strength between the gas-phase molecule CO and metallic surfaces. When experimental errors are considered, experimental results show that $E_{ad}(Pd) > E_{ad}(Pt) > E_{ad}(Rh) > E_{ad}(Ru) > E_{ad}(Ir)$ [$E_{ad}(Os)$ is absent in the author's knowledge [195–199]. However, the obtained E_{ad} values are hard to compare because the known simulation results come from different functionals. In addition, because relativistic effects into the core are neglected in the most previous calculations for CO adsorption on the above elements, the state-of-the-art DFT fails to predict the correct site preferences for CO/Pt(111) and CO/Rh(111) systems [173, 200, 201] because the relativistic effects lead to sizable modifications on bonding properties of these elements. After considering the relativistic effects into the core, the DFT results correspond to available experimental and theoretical results very well [202].

Transition metal clusters have potential use as catalysts in many important reactions, such as oxidation and hydrogenation [203–207]. Recent experiments revealed that the activity of small metallic clusters is extremely sensitive to their sizes [208–213]. As we all know, the properties of small clusters significantly differ from those of their corresponding bulk crystals, which can be attributed in part to the variation of the surface/volume ratio. This behavior has motivated investigators to propose new approaches to control catalysis by adjusting cluster size [203]. Thus, systematic study of the properties of a sequential growth of clusters can provide important fundamental insight into the mechanisms that govern catalysis [214, 215]. On CO/Au clusters systems, the odd–even vibrational phenomenon for E_{ad} values has been detected [216], with $55 < n < 146$ [217], which could be induced by an inadequate representation of the surface electronic structure in these cluster models [218]. For pyramidal Cu clusters, E_{ad} values of CO are also determined by the layer numbers l, which may be attributed to the cluster deformation [219].

3.3.1 CO adsorbed on the surface of transition metals

The $E_{ad}(Rh)$ value of the most favorable atop adsorption site for the CO/Rh(111) system is similar to experimental results, followed by the HCP, FCC, and bridge sites. For free gas, the determined $d_{C-O} = 1.15$ Å is 1.7% larger than experimental results [220]. For the atop adsorption system after a full relaxation, $d_{C-O} = 1.17$ Å and $d_{C-Rh} = 1.86$ Å, which correspond to experimental data of $d_{C-O} = 1.20 \pm 0.05$ Å and $d_{C-Rh} = 1.87 \pm 0.04$ Å well [221]. $d_{atop} < d_{bridge} < d_{hollow}$, that is, d is reversely proportional to E_{ad}. Because CO molecules affect only substrate atoms around their local environments, d_{C-O} and d_{M-C} values increase with the coordination because of the larger occupation of electrons in the $2\pi^*$ orbital [201]. For the CO/Os(0001) system, the order of favorable adsorption sites is atop > HCP > bridge in terms of the determined E_{Os} values with $d_{atop} < d_{bridge} < d_{HCP}$. The metallic surface atoms interacting with CO move outward from the surface, as hoped [192]. In addition, d_{C-O} is slightly elongated compared to that of the free gas due to back-donation of substrate electrons into a previously unoccupied anti-bonding CO-$2\pi^*$ orbital, which weakens the C–O bond. The calculated E_{ad} values of the most favorable site of CO/M systems, as shown in Table 3, have an order of $E_{ad}(Pd) > E_{ad}(Pt) > E_{ad}(Rh) > E_{ad}(Ru) > E_{ad}(Os) > E_{ad}(Ir)$, which is similar to the sequence of experimental results.

Table 3 Comparison among calculated E_1 values in eV on the most favorable site, other simulation results E_2 [201], E_3 [222, 223], and E_4 [224], and experimental results E_5 [195–199]. *es* denotes the electronic structure, d is the bond length in Å, and the subscript M indicates metallic element. Reprinted in part with permission from Ref. [202]. Copyright © 2007 American Chemical Society.

	es	Site	$-E_1$	$-E_2^{b}$	$-E_3^{c}$	$-E_4^{d}$	$-E_5$	d_{C-M}	d_{C-O}
Rh[a]	$4d^85s^1$	Atop	1.71	1.55	1.56	1.67	1.65 [194]	1.86	1.17
Rh	$4d^85s^1$	Bridge	1.56	1.48	1.41	1.58		2.04	1.19
Rh	$4d^85s^1$	FCC	1.57	1.50	1.38			2.13	1.20
Rh	$4d^85s^1$	HCP	1.62	1.59	1.47	1.64		2.11	1.20
Os[a]	$5d^66s^2$	Atop	2.02					1.92	1.17
Os	$5d^66s^2$	Bridge	1.45					2.11	1.19
Os	$5d^66s^2$	HCP	1.48					2.17	1.21
Ru	$4d^75s^1$	Atop	1.80	1.69			1.66 [198]	1.90	1.17
Pd	$4d^{10}5s^0$	FCC	1.35	1.68		1.60	1.30 [196]	2.12	1.19
Ir	$5d^76s^2$	Atop	2.12	1.64			>1.96 [199]	1.85	1.17
Pt	$5d^96s^1$	Atop	1.68	1.34	1.72, 1.39	1.56	1.66 [197]	1.84	1.16

[a] *es* denotes the electronic structure, d is the bond length in angstroms, and the subscript M indicates metallic element.
[b] For Rh and Os, simulated E values at different adsorption sites are shown.
[c] E_2 is calculated with the usual GGA-RPBE method without AER [201].
[d] E_3 is determined by the molecular GGA+U method [222, 223].
[e] E_4 is determined by extrapolating the values of the chemisorption energies obtained first from the usual GGAPBE method [224].

For comparison purposes, a DOS plot of six CO/M systems is determined and shown in Fig. 10. The electronic states of free CO in the systems are lowered in energy after binding to substrates, and the electron states of substrates are also changed remarkably to hybridize with CO molecules, except Pd(111). For CO/Pt(111) and CO/Pd(111) systems, the CO-2π* peak broadens and overlaps with the 1π orbital, and the interaction between CO-2π* and M-(5dxz+5dyz) orbitals leads to a hybrid orbital at higher energetic level around 2.5 eV. Because the anti-bonding dipole CO-2π* orbital is formed by the production of a nonbonding band that polarizes electrons of the neighboring atoms, the anti-bonding band disappears correspondingly when lone pair electrons transfer to a metallic surface [225]. This phenomenon can also be observed for Ir, Os, Ru, and Rh adsorption systems.

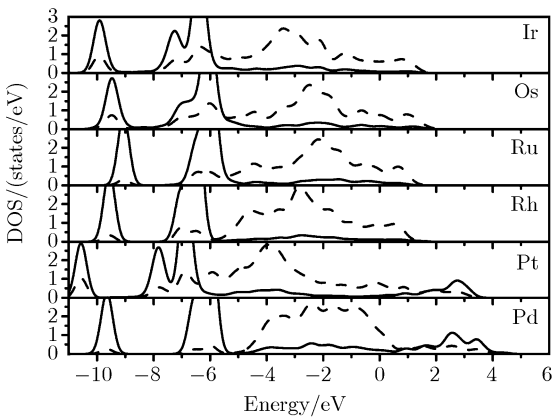

Fig. 10 DOS plot for CO/M systems at the preferred site. The solid and dashed lines indicate the states of CO and metals, respectively. The Fermi level is located at 0 eV. Reprinted in part with permission from Ref. [202]. Copyright © 2007 American Chemical Society.

3.3.2 CO adsorbed on Cu pyramidal clusters

The calculated E_{ad} values, and the corresponding geometry parameters, for CO, on Cu clusters are given in Table 4. For the CO/Cu adsorption system, two-layer Cu has the lowest E_{ad} value and thus exhibits the largest adsorption ability. Then, E_{ad} increases as l increases from 3 to 5, where $E_{ad1}(l) = -1.18$, –0.94, and –0.92 eV/atom, respectively. However, E_{ad1} values decrease to –1.01 and –1.03 eV/atom when $l = 6$ and 7. In general, the binding strength, or $-E_{ad}$, is inversely proportional to its corresponding d value between the adsorbate and the substrate [226]. This is our case as shown in Table 4 where the trend of $d_{1C-Cu} \propto E_{ad1}$. Thus, our "abnormal" E_{ad} value corresponds to their corresponding d_{1C-Cu} values. Compared with the experimental results, $d_{C-Cu} = 1.91$ Å for CO on Cu(111) surfaces [227] is much larger than our d_{1C-Cu} values, which confirms that CO binds more strongly on small clusters. In addition, the d_{1C-O} values slightly increase from 1.13 to 1.15 Å for all clusters in Table 4. It is well known that the binding between CO and low-index Cu surfaces are weak [228]. Recent experimentally determined heat of adsorption for the CO/Cu(111) system was reported to be –0.49 eV/atom [229], which is much larger than the E_{ad1} values listed in Table 4. Thus, the binding strength between CO and Cu can be significantly enhanced when size of Cu clusters is small. It is worth noting that our E_{ad} value for CO on 5-atom pyramidal Cu ($l = 2$) is 52.99% lower than $E_{ad} = -1.17$ eV/atom for CO on ground-state Cu_5 [230]. This is because an unstable cluster is more "eager" to adsorb small molecules to lower its free energy.

To look into the orbital hybridization conditions, the partial density of states (PDOS) charts for CO on four-layer Cu are calculated in Fig. 11. For comparison pur-

Table 4 Computed adsorption energy E_{ad} values in eV/atom and bond length d in Å for CO/Cu adsorption systems. The average bond length d_{ave} values of clean Cu clusters are also listed.

l	$-E_{ad1}$	d_{1C-Cu}	d_{1C-O}	d_{ave}	Δd^{a}_{ave}
2	1.72	1.79	1.15	2.45	0.11
3	1.18	1.81	1.15	2.50	0.06
4	0.94	1.83	1.15	2.54	0.02
5	0.92	1.84	1.15	2.56	0
6	1.01	1.82	1.15	2.57	0.01
7	1.03	1.82	1.15	2.58	0.02

[a] $\Delta d_{ave} = |d_{ave} - d_{bulk}|$, where $d_{bulk} = 2.56$ Å is the nearest atomic distance of bulk Cu.

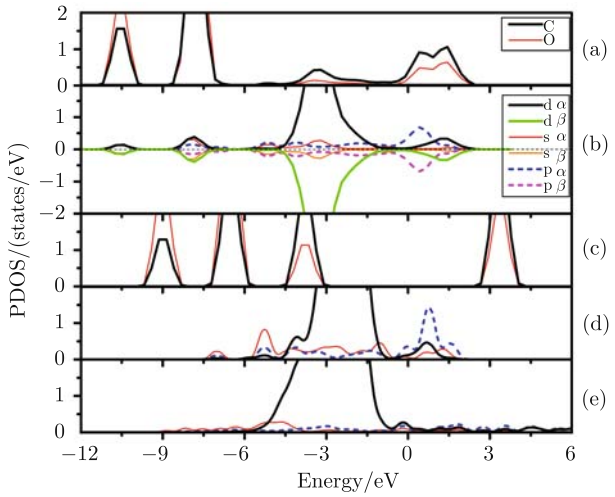

Fig. 11 PDOS plots of CO on four-layer Cu cluster: **(a)** Adsorbed CO, **(b)** Adsorbed Cu cluster where both spin-up (α) and spin-down (β) states are depicted, **(c)** Free CO, **(d)** Clean Cu cluster, and **(e)** Bulk Cu. The Fermi level is located at 0 eV. Reprinted in part with permission from Ref. [219]. Copyright © 2008 American Chemical Society.

poses, plots of free CO molecule, clean Cu cluster, and bulk Cu crystal are also depicted in Fig. 11. For a free CO, the orbitals of 4σ, 1π, 5σ, and $2\pi^*$ are localized at about –8.99 eV, –6.57 eV, –3.77 eV, and 3.47 eV, respectively. Compared with Fig. 11(c), the states of adsorbed CO move largely to a lower energy range, where the 4σ orbital is still localized, while the 5σ and 1π orbitals broaden and dominate the interaction [see Fig. 11(a)]. Both the contributions from spin-up (α) and spin-down (β) states for adsorbed Cu are plotted in Fig. 11(b), from which it is discernable that β is identical to α, except the spin direction. This consists of the conditions of the HOMO (highest occupied molecular orbitals) and LUMO (lowest unoccupied molecular orbitals) orbitals for CO on small Cu clusters [226]. Comparing Fig. 11(a) with Fig. 11(b), not only d but also s and p states of Cu hybridize strongly with those of adsorbed CO. Thus, a new bond is formed between C and Cu due to the charge transfer between them. The states of the Cu cluster after adsorption move left in comparison with those of the clean Cu cluster [see Fig. 11(d)]. This implies that the stability increases when small molecules are adsorbed. Notably, the band of bulk Cu is dominated by the d orbital, and very weak p state can be seen in Fig. 11(e). Interestingly, large contributions from $s$and p orbitals can be detected in the PDOS plot for clean Cu cluster. Among them, the p state becomes especially intensive for the orbitals above the Fermi level as shown in Fig. 11(d). Thus, the Cu cluster has stronger adsorption ability than that of the bulk Cu crystal where the former owns more empty orbitals to accept the charges from the CO molecule.

4 Concluding remarks

Using DFT calculations, several theoretical models corresponding to the actually applied catalysts are established. The reaction mechanisms for the catalytic cycle including the associated barriers, the reactive energies, the intermediates, and the transient states are achieved, which are in good agreement with experimental measurements. In addition, the adsorption properties of several representative systems are also calculated. The outcome may help us to elucidate the fundamental aspects of the reaction chemistry at the molecular and electronic levels. It can be found that DFT is powerful and plays an important role in the research of surface catalysis, which is helpful in the design of new materials and catalysts.

Most of the reactants and reaction steps cited in this review are relatively simple, a reflection of the state of the field. In spite of their limitations, these studies have furnished much in-depth understanding of reactions, such as oxidative additions, hydride, and reductive eliminations, and have impacted the design and manipulation of catalysts. Collectively, the surface science studies carried out so far have furnished a useful database for the chemistry of organic molecules and fragments on a variety of solid surfaces and have identified important trends in reactivity and selectivity. Nevertheless, this field is in its infancy; in the future, and in parallel to adding complexity to the model used for the catalyst, more effort is needed to study the mechanistic details of complex reactions. The next decades are expected to not only enrich the existing knowledge but also significantly advance the molecular-level understanding of the surface chemistry of more realistic systems.

Acknowledgements The authors acknowledge the financial supports from the National Key Basic Research and Development Program of China (Grant No. 2004CB619301) and "985 Project" of Jilin University.

References

1. N. López, M. García-Mota, and J. Gómez-Díaz, J. Phys. Chem. C, 2008, 112: 247

2. W. K. Offermans, A. P. J. Jansen, and R. A. van Santen, Surf. Sci., 2006, 600: 1714
3. M. Baerns, A. Imbihl, V. A. Kondratenko, R. Kraehnert, W. K. Offermans, R. A. van Santen, and A. Scheibe, J. Catal., 2005, 232: 226
4. L. Hannevold, O. Nilsen, A. Kjekshus, and H. Fjellvåg, Appl. Catal. A, 2005, 284: 185
5. G. Novell-Leruth, A. Valcárcel, A. Clotet, J. M. Ricart, and J. Pérez-Ramírez, J. Phys. Chem. B, 2005, 109: 18061
6. Z. F. Zhao, Z. J. Wu, L. X. Zhou, M. H. Zhang, W. Li, and K. Y. Tao, Catal. Commun., 2008, 9: 2191
7. M. Jacquin, D. J. Jones, J. Rozière, S. Albertazzi, A. Vaccari, M. Lenarda, L. Storaro, and R. Ganzerla, Appl. Catal. A, 2003, 251: 131
8. C. Milone, G. Neri, A. Donato, M. G. Musolino, and L. Mercadante, J. Catal., 1996, 159: 253
9. C. N. Rowley and T. K. Woo, J. Am. Chem. Soc., 2008, 130: 7218
10. B. L. Edelbach, D. A. Vicic, R. J. Lachicotte, and W. D. Jones, Organometallics, 1998, 17: 4784
11. H. Lesnard, M. L. Bocquet, and N. Lorente, J. Am. Chem. Soc., 2007, 129: 4298
12. W. Gao, W. T. Zheng, and Q. Jiang, J. Chem. Phys., 2008, 129: 164705
13. S. Linic and M. A. Barteau, J. Catal., 2003, 214: 200
14. W. Gao, M. Zhao, and Q. Jiang, J. Phys. Chem. C, 2007, 111: 4042
15. S. Linic and M. A. Barteau, J. Am. Chem. Soc., 2003, 125: 4034
16. S. Linic and M. A. Barteau, J. Am. Chem. Soc., 2002, 124: 310
17. M. L. Bocquet, A. Michaelides, D. Loffreda, P. Sautet, A. Alavi, and D. A. King, J. Am. Chem. Soc., 2003, 125: 5620
18. L. Guczi, G. Stefler, O. Geszti, Z. Koppány, Z. Kónya, É. Molnár, M. Urbán, and I. Kiricsi, J. Catal., 2006, 244: 24
19. L. Olsson and B. Andersson, Topics in Catalysis, 2004, 28: 89
20. Y. Sakamoto, K. Okumura, Y. Kizaki, S. Matsunaga, N. Takahashi, and H. Shinjoh, J. Catal., 2006, 238: 361
21. P. Hohenberg and W. Kohn, Phys. Rev., 1964, 136: B864
22. W. Kohn and L. J. Sham, Phys. Rev., 1965, 140: A1133
23. G. Kresse and J. Fürthmuller, Comput. Mater. Sci., 1996, 6: 15
24. B. Delley. J. Chem. Phys., 1990, 92: 508
25. B. Delley, J. Chem. Phys., 2000, 113: 7756
26. M. D. Segall, P. J. D. Lindan, M. J. Probert, C. J. Pickard, P. J. Hasnip, S. J. Clark, and M. C. Payne, J. Phys.: Condens. Matter, 2002, 14: 2717
27. The help of the Materials studio modeling
28. G. Henkelman, B. Uberuaga, and H. Jonsson, J. Chem. Phys., 2000, 113, 9901
29. S. Meng, E. Wang, C. Frischkorn, M. Wolf, and S. Gao, Chem. Phys. Lett., 2005, 402: 384
30. J. J. Cowell, A. K. Santra, R. Lindsay, R. M. Lambert, A. Baraldi, and A. Goldoni, Surf. Sci., 1999, 437: 1
31. A. K. Santra, J. J. Cowell, and R. M. Lambert, Catal. Lett., 2000, 67: 87
32. R. A. van Santen and H. P. C. E. Kuipers, Adv. Catal., 1987, 35: 265
33. B. S. Bal'zhinimaev, Kinet. Catal., 1999, 40: 795
34. C. T. Campbell, Surf. Sci., 1985, 157: 43
35. C. T. Campbell, Surf. Sci., 1986, 173: L641
36. A. Raukema, D. A. Butler, F. M. A. Box, and A. W. Kleyn, Surf. Sci., 1996, 347: 151
37. S. R. Bare, K. Griffiths, W. N. Lennard, H. T. Tang, Surf. Sci., 1995, 342: 185
38. C. I. Carlisle, D. A. King, M. L. Bocquet, J. Cerda, and P. Sautet, Phys. Rev. Lett., 2000, 84: 3899
39. C. I. Carlisle, T. Fujimoto, W. S. Sim, and D. A. King, Surf. Sci., 2000, 470: 15
40. R. A. van Santen and C. P. M. de Groot, J. Catal., 1986, 98: 530
41. X. Bao, M. Muhler, Th. Schedel-Niedrig, and R. Schlögl, Phys. Rev. B, 1996, 54: 2249
42. D. Stacchiola, G. Wu, M. Kaltchev, W. T. Tysoe, Surf. Sci., 2001, 486: 9
43. S. R. Bare, J. Vac. Sci. Technol. A, 1992, 10: 2336
44. G. Wu, D. Stacchiola, M. Collins, and W. T. Tysoe, Surf. Rev. Lett., 2000, 7: 271
45. E. M. Stuve, R. J. Madix, and B. A. Sexton, Surf. Sci., 1981, 111: 11
46. C. T. Campbell and M. T. Paffett, Surf. Sci., 1984, 143: 517
47. G. S. Jones, M. Mavrikakis, M. A. Barteau, and J. M. Vohs, J. Am. Chem. Soc., 1998, 120: 3196
48. G. Wu, D. Stacchiola, M. Kaltchev, and W. T. Tysoe, Surf. Sci., 2000, 463: 81
49. V. I. Bukhtiyarov, A. I. Boronin, and V. I. Savchenko, J. Catal., 1994, 150: 262
50. C. Henriques, M. F. Portela, and C. Mazzocchia, in: New Developments in Selective Oxidation II, V. C. Corberan and S. V. Bellon (Eds.), Amsterdam: Elsevier Science, 1994: 499
51. G. H. Twigg, Proc. R. Soc. A, 1946, 188: 92
52. C. T. Campbell, J. Catal., 1985, 94: 436
53. J. K. Norskov, Nature, 2001, 414: 405
54. P. A. Kilty and W. M. H. Sachtler, Catal. Rev. Sci. Eng., 1974, 10: 1
55. H. H. Voge and C. R. Adams, Adv. Catal., 1967, 17: 151
56. M. I. Temkin, Adv. Catal., 1979, 28: 173
57. C. T. Campbell, J. Catal., 1986, 99: 28
58. G. Rovida, F. Pratesi, M. Maglietta, and E. Ferroni, Surf. Sci., 1974, 43: 230
59. C. I. Carlisle and D. A. King, Phys. Rev. Lett., 2000, 84: 3899
60. A. Michaelides, K. Reuter, and M. J. Scheffler, Vac. Sci. Technol. A, 2005, 23: 1487
61. J. Schnalt, A. Michaelides, J. Knudsen, R. T. Vang, K. Reuter, E. Lægsgaard, M. Scheffler, and F. Besenbacher, Phys. Rev. Lett., 2006, 96: 146101
62. M. Schmid, A. Reicho, A. Stierle, I. Costina, J. Klikovits, P. Kostelnik, O. Dubay, G. Kresse, J. Gustafson, E. lundgren, J. N. Andersen, H. Dosch, and P. Varga, Phys. Rev. Lett., 2006, 96: 146102
63. C. T. Campbell and B. E. Koel, J. Catal., 1985, 92: 272
64. L. Petrov, A. Eliyas, C. Maximov, and D. Shopov, Appl. Catal., 1988, 41: 23
65. J. K. Nørskov, T. Bligaard, A. Logadottir, S. Bahn, L. B. Hansen, M. Bollinger, H. Bengaard, B. Hammer, Z. Slji-

vancanin, M. Mavrikakis, Y. Xu, S. Dahl, and C. J. H. Jacobsen, J. Catal., 2002, 209: 275
66. M Saeys, M. F. Reyniers, G. B. Marin, and M. Neurock, J. Phys. Chem. B, 2002, 106: 7489
67. M. Saeys, M. F. Reyniers, M. Neurock, and G. B. Marin, J. Phys. Chem. B, 2003, 107: 3844
68. C. Morin, D. Simon, and P. Sautet, J. Phys. Chem. B, 2004, 108: 5653
69. P. G. Wenthold, Angew. Chem. Int. Ed., 2005, 44: 7170
70. C. J. Barnes, M. Valden, and M. Pessa, Surf. Rev. Lett., 2000, 1: 67
71. C. Morin, D. Simon, and P. Sautet, J. Phys. Chem. B, 2004, 108: 12084
72. C. Morin, D. Simon, and P. Sautet, J. Phys. Chem. B, 2003, 107: 2995
73. Y. G. Kim, J. E. Soto, X. L. Chen, Y. S. Park, and M. P. Soriaga, J. Electroanal. Chem., 2003, 554: 167
74. S. Z. Zou, C. T. Williams, E. K. Y. Chen, and M. J. Weaver, J. Am. Chem. Soc., 1998, 120: 3811
75. L. J. Wan, C. Wang, C. L. Bai, and M. Osawa, J. Phys. Chem. B, 2001, 105: 8399
76. S. Haq and D. A. King, J. Phys. Chem., 1996, 100: 16957
77. M. Xi, M. X. Yang, S. K. Jo, and B. E. Bent, J. Chem. Phys., 1994, 101: 9122
78. T. Munakata, J. Chem. Phys., 1999, 110: 2736
79. M. W. Howard and R. P. Cooney, Chem. Phys. Lett., 1982, 87: 299
80. R. A. Wolkow and M. Moskovits, J. Chem. Phys., 1992, 96: 3966
81. M. Litorja, C. L. Haynes, A. J. Haes, T. R. Jensen, and R. P. Van duyne, J. Phys. Chem. B, 2001, 105: 6907
82. D. Syomin, J. Kim, B. E. Koel, and G. B. Ellison, J. Phys. Chem. B, 2001, 105: 8387
83. P. Gao and M. J. Weaver, J. Phys. Chem., 1985, 89: 5040
84. B. E. Koel, J. E. Crowell, B. E. Bent, C. M. Mate, and G. Somorjai. A., J. Phys. Chem., 1986, 90: 2949
85. A. Clotet, J. M. Ricart, F. Illas, G. Pacchioni, and R. M. Lambert, J. Am. Chem. Soc., 2000, 122: 7573
86. A. Nilsson, M. Weinelt, T. Wiell, P. Bennich, O. Karis, N. Wassdahl, J. Stöhr, and M. G. Samant, Phys. Rev. Lett., 1997, 78: 2847
87. M. Weinelt, N. Wassdahl, T. Wiell, O. Karis, J. Hasselström, P. Bennich, A. Nilsson, J. Stöhr, and M. Samant, Phys. Rev. B, 1998, 58: 7351
88. H. Koschel, G. Held, P. Trischberger, W. Widdra, and H. P. Steinrück, Surf. Sci., 1999, 437: 125
89. L. Triguero, L. G. M. Pettersson, B. Minaev, and H. Agren, J. Chem. Phys., 1998, 108: 1193
90. L. J. Lauhon and W. Ho, J. Phys. Chem. A, 2000, 104: 2463
91. L. J. Lauhon and W. Ho, Surf. Sci., 2000, 451: 219
92. P. S. Weiss, M. M. Kamma, T. M. Graham, and S. J. Stranick, Langmuir, 1998, 14: 1284
93. B. E. Bent, Chem. Rev. (Washington, D. C.), 1996, 96: 1361
94. S. Haq and D. A. King, J. Phys. Chem., 1996, 100: 16957
95. M. C. Tsai and E. L. Muetterties, J. Am. Chem. Soc., 1982, 104: 2534
96. A. Wander, G. Held, R. Q. Hwang, G. S. Blackman, M. L. Xu, P. de Andres, M. A. Hove Van, and G. A. Somorjai, Surf. Sci., 1991, 249: 21
97. G. K. Liu, B. Ren, D. Y. Wu, S. Duan, Ji. F. Li, J. L. Yao, R. A. Gu, and Z. Q. Tian, J. Phys. Chem. B, 2006, 110: 17498
98. K. Pussi, M. Lindroos, and J. C. Barnes, Chem. Phys. Lett., 2001, 341: 7
99. D. Majumdar, S. Roszak, and K. Balasubramanian, J. Chem. Phys., 2001, 114: 10300
100. E. S. Kryachko, A. V. Arbuznikov, and M. F. A. Hendrickx, J. Phys. Chem. B, 2001, 105: 3557
101. M. T. de M. Cruz, J. W. de M. Carneiro, D. A. G. Aranda, and M. Bühl, J. Phys. Chem. C, 2007, 111: 11076
102. J. M. Campbell, S. Seimanides, and C. T. Campbell, J. Phys. Chem., 1989, 93: 815
103. L. T. Ngo, L. J. Xu, A. W. Grant, and C. T. Campbell, J. Phys. Chem. B, 2003, 107: 1174
104. F. S. Thomas, N. S. Chen, L. P. Ford, and R. I. Masel, Surf. Sci., 2001, 486: 1
105. T. E. Fischer, S. R. Kelemen, and H. P. Bonzel, Surf. Sci., 1977, 64: 157
106. B. E. Koel, J. E. Crowell, B. E. Bent, C. M. Mate, and G. A. Somorjai, J. Phys. Chem., 1986, 90: 2949
107. H. Cabibil, H. Ihm, and J. M. White, Surf. Sci., 2000, 447: 91
108. M. L. Bocquet, H. Lesnard, and N. Lorente, Phys. Rev. Lett., 2006, 96: 096101
109. The separating H rather lies in a pseudo-bridge position than in a strict on top position
110. D. Loffreda, F. Delbecq, F. Vigné, and P. Sautet, J. Am. Chem. Soc., 2006, 128: 1316
111. T. Komeda, Y. Kim, Y. Sainoo, and M. Kawai, J. Chem. Phys., 2004, 120: 5347
112. K. M. Erwin and V. F. DeTuri, J. Phys. Chem. A, 2002, 106: 9947
113. L. J. Lauhon and W. Ho, J. Phys. Chem. A, 2000, 104: 2463
114. S. Venkataramani, M. Winkler, and W. Sander, Angew. Chem., 2005, 117: 6464
115. S. Venkataramani, M. Winkler, and W. Sander, Angew. Chem. Int. Ed., 2005, 44: 6306
116. M. B. Hugenschmidt, A. L. Diaz, and C. T. Campbell, J. Phys. Chem., 1992, 96: 5974
117. C. T. Campbell, J. M. Campbell, P. J. Dalton, F. C. Henn, J. A. Rodriguez, and S. G. Seimanides, J. Phys. Chem., 1989, 93: 806
118. A. M. C. Cristian, Y. H. Shao, and A. I. Krylov, J. Phys. Chem. A, 2004, 108: 6581
119. N. Lorente, M. F. G. Hedouin, R. E. Palmer, and M. Persson, Phys. Rev. B, 2003, 68: 155401
120. Z. Ma and F. Zaera, Surf. Sci. Rep., 2006, 61: 229
121. B. C. Stipe, M. A. Rezaei, and W. Ho, Science, 1998, 280: 1732
122. G. Kyriakou, J. Kim, M. S. Tikhov, N. Macleod, and R. M. Lambert, J. Phys. Chem. B, 2005, 109: 10952
123. J. W. Medlin and M. D. Allendorf, J. Phys. Chem. B, 2003, 107: 217

124. J. Dvorak and J. Hrbek, J. Phys. Chem. B, 1998, 102: 9443
125. C. G. P. M. Bernardo, and G. A. N. F. Gomes, J. Mol. Struct., 2003, 629: 251
126. N. Mingo and K. Makoshi, Phys. Rev. Lett., 2000, 84: 3694
127. D. Arvanitis, L. Wenzel, and K. Baberschke, Phys. Rev. Lett., 1987, 59: 2435
128. X. F. Hu, C. J. Chen, and T. C. Tang, Surf. Sci., 1996, 365: 319
129. B. S. Stipe, M. A. Razaei, and W. Ho, Phys. Rev. Lett., 1999, 82: 1724
130. B. C. Stipe, M. A. Razaei, and W. Ho, Phys. Rev. Lett., 1998, 81: 1263
131. Y. Konishi, Y. Sainoo, K. Kanazawa, S. Yoshida, A. Taninaka, O. Takeuchi, and H. Shigekawa, Phys. Rev. B, 2005, 71: 193410
132. S. Bao, K. M. Schindler, P. Hofmann, V. Fritzsche, A. B. Bradshaw, and D. P. Woodruff, Surf. Sci., 1994, 291: 295
133. D. A. Outka, C. M. Friend, S. Jorgensen, and R. J. Madix, J. Am. Chem. Soc., 1983, 105: 3468
134. N. R. Avery, J. Am. Chem. Soc., 1985, 107: 6712
135. H. Öström, D. Nordlund, H. Ogasawara, K. Weiss, L. Triguero, L. G. M. Pettersson, and A. Nilsson A., Surf. Sci., 2004, 565: 206
136. L. F. Yuan, J. Yang, Q. Li, and Q. S. Zhu, J. Chem. Phys., 2002, 116: 3104
137. F. E. Olsson, M. Persson, N. Lorente, L. J. Lauhon, and W. Ho, J. Phys. Chem. B, 2002, 106: 8161
138. F. E. Olsson, M. Persson, N. Lorente, L. J. Lauhon, and W. Ho, J. Phys. Chem. B, 2002, 106: 11073
139. M. Witko and K. Hermann, Appl. Catal. A, 1998, 172: 85
140. K. Hermann and M. Witko, Surf. Sci., 1995, 337: 205
141. W. Liu, J. S. Lian, and Q. Jiang, J. Phys. Chem. C, 2007, 111: 18189
142. B. C. Stipe, M. A. Rezaei, and W. Ho, Science, 1998, 280: 1732
143. B. C. Stipe, M. A. Rezaei, and W. Ho, Phys. Rev. Lett., 1999, 82: 1724
144. L. Triguero, L. G. M. Petterson, B. Minaev, and H. Agren, J. Chem. Phys., 1998, 108: 1193
145. D. Arvanitis, U. Dübler, L. Wenzel, K. Baberschke, and J. Stühr, Surf. Sci., 1986, 178: 696
146. X. F. Hu, C. J. Chen, and J. C. Tang, Surf. Sci., 1996, 365: 319
147. N. Lorente and M. Persson, Phys. Rev. Lett., 2000, 85: 2997
148. D. Fuhrmann, D. Wacker, K. Weiss, K. Hermann, M. Witko, and Ch. Wöll, J. Chem. Phys., 1998, 108: 2651
149. Q. Jiang, H. M. Lu, and M. Zhao, J. Phys.: Condens. Matter, 2004, 16: 521
150. Ch. Wöll, K. Weiss, and P. S. Bagus, Chem. Phys. Lett., 2000, 332: 553
151. N. M. Marković and Jr. P. N. Ross, Surf. Sci. Rep., 2002, 45: 11
152. Y. X. Chen, A. Miki, S. Ye, H. Sakai, M. Osawa, J. Am. Chem. Soc., 2003, 125: 3680
153. J. Greeley and M. Mavrikakis, J. Am. Chem. Soc., 2004, 126: 3910
154. W. Vielstich and X. H. Xia, J. Phys. Chem., 1995, 99: 10421
155. E. Herrero, W. Chrzanowski, and A. Wieckowski, J. Phys. Chem., 1995, 99: 10423
156. G. Q. Lu, W. Chrzanowski, and A. Wieckowski, J. Phys. Chem. B, 2000, 104: 5566
157. T. D. Jarvi, S. Sriramulu, and E. M. Stuve, J. Phys. Chem. B, 1997, 101: 3649
158. R. Parsons and T. VanderNoot, J. Electroanal. Chem. 1988, 257: 9
159. B. Beden, C. Lamy, A. Bewick, and K. Kunimatsu, J. Electroanal. Chem., 1981, 121: 343
160. T. H. M. Housmans, A. H. Wonders, and M. T. M. Koper, J. Phys. Chem. B, 2006, 110: 10021
161. B. Beden, J. M. Leger, C. Lamy in Modern Aspects of Electrochemistry, Vol. 22, edited by J. O. M. Bockris, R. E. White, and B. E. Conway, New York, 1992: 97
162. Y. Zhu, H. Uchida, T. Yajima, and M. Watanabe, Langmuir, 2001, 17: 146
163. M. Nakamura, K. Shibutani, and N. Hoshi, Chem PhysChem, 2007, 8: 1846
164. D. Cao, G. Q. Lu, A. Wieckowski, S. A. Wasileski, and M. Neurock, J. Phys. Chem. B, 2005, 109: 11622
165. A. Cuesta, J. Am. Chem. Soc., 2006, 128: 13332
166. W. Gao, M. Zhao, and Q. Jiang, ChemPhysChem, 2008, 9: 2092
167. J. Greeley and M. Mavrikakis, J. Am. Chem. Soc., 2002, 124: 7193
168. S. K. Desai, M. Neurock, and K. Kourtakis, J. Phys. Chem. B, 2002, 106: 2559
169. X. Q. Gong, P. Hu, and R. Raval, J. Chem. Phys., 2003, 119: 6324
170. M. Endo, T. Matsumoto, J. Kubota, K. Domen, and C. Hirose, J. Phys. Chem. B, 2001, 105: 1573
171. M. Endo, T. Matsumoto, J. Kubota, K. Domen, and C. Hirose, J. Phys. Chem. B, 2000, 104: 4916
172. T. D. Jarvi and E. M. Stuve, Electrocatalysis, edited by J. Lipkowski and P. N. Ross, Germany, Heidelberg: Wiley-VCH, 1998: 75
173. H. Orita, N. Itoh, and Y. Inada, Chem. Phys. Lett., 2004, 384: 271
174. R. Rajasree, J. H. B. J. Hoebink, and J. C. Schouten, J. Catal., 2004, 223: 36
175. D. Curulla, A. Govender, T. C. Bromfield, and J. W. Niemantsverdriet, J. Phys. Chem. B, 2006, 110: 13897
176. R. A. Olsen, P. H. T. Philipsen, and E. J. Baerends, J. Chem. Phys., 2003, 119: 4522
177. M. Gajdoš, A. Eichler, J. Hafner, G. Meyer, and K. H. Rieder, Phys. Rev. B, 2005, 71: 035402
178. J. A. Steckel, A. Eichler, and J. Hafner, Phys. Rev. B, 2003, 68: 085416
179. M. Mavrikakis, J. Rempel, J. Greeley, L. B. Hansen, and J. K. Nørskov, J. Chem. Phys., 2002, 117: 6737
180. R. He, H. Kusaka, M. Mavrikakis, and J. A. Dumesic, J. Catal., 2003, 217: 209
181. S. Gonzalez and F. Illas, Surf. Sci., 2005, 598: 144
182. C. Song, Q. Ge, and L. Wang, J. Phys. Chem. B, 2005, 109: 22341
183. A. Gil, A. Clotet, J. M. Ricart, F. Illas, B. Álvarez, A.

Rodes, and J. M. Feliu, J. Phys. Chem. B, 2001, 105: 7263
184. A. Eichler, Phys. Rev. B, 2005, 71: 125418
185. D. Curulla, A. Clotet, J. M. Ricart, and F. Illas, J. Phys. Chem. B, 1999, 103: 5246
186. I. N. Remediakis, N. Lopez, and J. K. Nørskov, Appl. Catal. A, 2005, 291: 13
187. L. M. Molina and B. Hammer, Phys. Rev. B, 2004, 69: 155424
188. L. B. Liu, B. McAllister, H. Q. Ye, and P. Hu, J. Am. Chem. Soc., 2006, 128: 4017
189. H. S. Gandhi, G. W. Graham, and R. W. McCabe, J. Catal., 2003, 216: 433
190. A. Alavi, P. Hu, T. Deutsch, P. L. Silvestrelli, and J. Hutter, Phys. Rev. Lett., 1998, 80: 3650
191. B. Narloch, G. Held, and D. Menzel, Surf. Sci., 1995, 340: 159
192. G. Krenn, I. Bako, and R. Schennach, J. Chem. Phys., 2006, 124: 144703
193. S. Schwegmann, H. Over, V. De Renzi, and G. Ertl, Surf. Sci., 1997, 375: 91
194. D. J. Liu and J. W. Evans, J. Chem. Phys., 2006, 124: 154705
195. M. J. P. Hopstaken and J. W. Niemantsverdriet, J. Chem. Phys., 2000, 113: 5457
196. X. Guo and J. T. Jr. Yates, J. Chem. Phys., 1989, 90: 6761
197. Y. Y. Yeo, L. Vattuone, and D. A. King, J. Chem. Phys., 1997, 106: 392
198. H. Pfnür, P. Feulner, and D. Menzel, J. Chem. Phys., 1983, 79: 4613
199. C. M. Comrie and W. H. Weinberg, J. Chem. Phys., 1976, 64: 250
200. P. J. Feibelman, B. Hammer, J. K. Nørskov, F. Wagner, M. Scheffler, R. Stumpf, R. Watwe, and J. Dumesic, J. Phys. Chem. B, 2001, 105: 4018, and references therein
201. M. Gajdoš, A. Eichler, and J. Hafner, J. Phys.: Condens. Matter, 2004, 16: 1141
202. W. Liu, Y. F. Zhu, J. S. Lian, and Q. Jiang, J. Phys. Chem. C, 2007, 111: 1005
203. Z. Xu, F. S. Xiao, S. K. Purnell, Q. Alexeev, S. Kawi, S. E. Deutsch, and B. C. Gates, Nature, 1994, 372: 346
204. K. Jacobs, D. Zaziski, E. C. Scher, A. B. Herhold, and A. P. Alivisatos, Science, 2001, 293: 1803
205. G. H. Guvelioglu, P. Ma, X. He, R. C. Forrey, and H. Cheng, Phys. Rev. Lett., 2005, 94: 026103
206. M. Tada, T. Sasaki, and Y. Iwasawa, J. Catal., 2002, 211: 496
207. O. V. Safonova, H. Tromp, van J. A. Bokhoven, F. M. F. de Groot, J. Evans, and P. Glatzel, J. Phys. Chem. B, 2006, 110: 16162
208. F. Li and B. C. Gates, J. Phys. Chem. C, 2007, 111: 262
209. A. M. Argo, J. F. Odzak, and B. C. Gates, J. Am. Chem. Soc., 2003, 125: 7107
210. K. Bergamaski, A. L. N. Pinheiro, E. Teixeira-Neto, and F. C. Nart, J. Phys. Chem. B, 2006, 110: 19271
211. N. Semagina, A. Renken, and L. Kiwi-Minsker, J. Phys. Chem. C, 2007, 111: 13933
212. S. Panigrahi, S. Basu, S. Praharaj, S. Pande, S. Jana, A. Pal, S. K. Ghosh, and T. Pal, J. Phys. Chem. C, 2007, 111: 4596
213. J. P. Deng, W. C. Shih, and C. Y. Mou, ChemPhysChem, 2005, 6: 2021
214. R. C. Forrey, G. H. Guvelioglu, P. Ma, X. He, and H. Cheng, Phys. Rev. B, 2006, 73: 155437
215. G. H. Guvelioglu, P. Ma, X. He, R. C. Forrey, and H. Cheng, Phys. Rev. B, 2006, 73: 155436, and references therein
216. N. S. Phala, G. Klatt, and E. Van Steen, Chem. Phys. Lett., 2004, 395: 33
217. I. V. Yudanov, R. Sahnoun, K. M. Neyman, and N. Rösch, J. Chem. Phys., 2002, 117: 9887
218. K. Hermann, P. S. Bagus, and C. J. Nelin, Phys. Rev. B, 1987, 35: 9467
219. W. Liu, Y. H. Zhao, E. J. Lavernia, and Q. Jiang, J. Phys. Chem. C, 2008, 112: 7672
220. G. Kresse, A. Gil, and P. Sautet, Phys. Rev. B, 2003, 68: 073401
221. S. E. Mason, I. Grinberg, and A. M. Rappe, Phys. Rev. B, 2004, 69: 161401(R)
222. M. Gajdoš and J. Hafner, Surf. Sci., 2005, 590: 117
223. D. R. Lide, CRC Handbook of Chemistry and Physics, 81th Ed., Boca Raton, FL: CRC Press, 2000
224. M. Gierer, A. Barbieri, M. A. Van Hove, and G. A. Somorjai, Surf. Sci., 1997, 391: 176
225. H. L. Skriver and N. M. Rosengaard, Phys. Rev. B, 1992, 46: 7157
226. A. Poater, M. Duran, P. Jaque, A. Toro-Labbé, and M. Solà, J. Phys. Chem. B, 2006, 110: 6526
227. E. J. Moler, S. A. Kellar, W. R. A. Huff, Z. Hussain, Y. Chen, and D. A. Shirley, Phys. Rev. B, 1996, 54: 10862
228. S. Sakong, C. Mosch, and A. Groβ, Phys. Chem. Chem. Phys., 2007, 9: 2216
229. S. Vollmer, G. Witte, and C. Wöll, Catal. Lett., 2001, 77: 97
230. Z. Cao, Y. Wang, J. Zhu, W. Wu, and Q. Zhang, J. Phys. Chem. B, 2002, 106: 9649